Development of Three-Dimensional Anthropometric Models of Seated and Standing Children

Matthew P. Reed
Sheila M. Ebert
Byoung-Keon Daniel Park
Kathleen D. Klinich
Jonathan D. Rupp

University of Michigan Transportation Research Institute

UMTRI-2016-2

January 2016

Technical Report Documentation Page

1. Report No. UMTRI-2016-2	2. Government Accession No.	3. Recipient's Catalog No.
Development of Three-Dimensional Anthropometric Models of Seated and Standing Children		5. Report Date 6. Performing Organization Code
7. Author(s) Reed, M.P., Ebert, S.M., Park, B-K., Klinich, K.D., and Rupp, J.D.		8. Performing Organization Report No. UMTRI-2016-2
9. Performing Organization Name and Address University of Michigan Transportation Research Institute 2901 Baxter Rd. Ann Arbor MI 48109		10. Work Unit No. (TRAIS) 11. Contract or Grant No.
12. Sponsoring Agency Name and Address National Highway Traffic Safety Administration		13. Type of Report and Period Covered 14. Sponsoring Agency Code
15. Supplementary Notes		

16. Abstract

A laboratory study was conducted to develop statistical models of posture and body shape for children. Whole-body laser-scan data were obtained from 150 boys and girls ages 4 to 12 in a wide range of postures. Standard anthropometric measures were taken and additional three-dimensional body landmark locations were measured with the children sitting on a vehicle seat with and without a belt-positioning booster. A statistical analysis of the body scan data was conducted to develop models of standing and seated body shapes. The models are parameterized by stature, body weight, and erect sitting height, and torso recline and flexion can be adjusted in the seated model. The seated model outputs were compared with the scanned shapes of the Hybrid-III 6YO and 10YO ATDs. The largest discrepancies were noted in the upper thorax and lap areas. The data and models generated in this project will find a wide range of applications in crash safety, including providing guidance for the development of child dummies, computational models of children, and child restraint systems.

17. Key Word anthropometry, children, posture, body shape	18. Distribution Statement		
19. Security Classif. (of this report)	20. Security Classif. (of this page)	21. No. of Pages 56	22. Price

Metric Conversion Chart

APPROXIMATE CONVERSIONS TO SI UNITS

SYMBOL	WHEN YOU KNOW	MULTIPLY BY	TO FIND	SYMBOL
LENGTH				
In	inches	25.4	millimeters	mm
Ft	feet	0.305	meters	m
Yd	yards	0.914	meters	m
Mi	miles	1.61	kilometers	km
AREA				
in^2	squareinches	645.2	square millimeters	mm^2
ft^2	squarefeet	0.093	square meters	m^2
yd^2	square yard	0.836	square meters	m^2
Ac	acres	0.405	hectares	ha
mi^2	square miles	2.59	square kilometers	km^2
VOLUME				
fl oz	fluid ounces	29.57	milliliters	mL
gal	gallons	3.785	liters	L
ft^3	cubic feet	0.028	cubic meters	m^3
yd^3	cubic yards	0.765	cubic meters	m^3
NOTE: volumes greater than 1000 L shall be shown in m^3				
MASS				
oz	ounces	28.35	grams	g
lb	pounds	0.454	kilograms	kg
T	short tons (2000 lb)	0.907	megagrams (or "metric ton")	Mg (or "t")
TEMPERATURE (exact degrees)				
^oF	Fahrenheit	5 (F-32)/9 or (F-32)/1.8	Celsius	^oC
FORCE and PRESSURE or STRESS				
lbf	poundforce	4.45	newtons	N
lbf/in^2	poundforce per square	6.89	kilopascals	kPa

	inch			
LENGTH				
mm	millimeters	0.039	inches	in
m	meters	3.28	feet	ft
m	meters	1.09	yards	yd
km	kilometers	0.621	miles	mi
AREA				
mm^2	square millimeters	0.0016	square inches	in^2
m^2	square meters	10.764	square feet	ft^2
m^2	square meters	1.195	square yards	yd^2
ha	hectares	2.47	acres	ac
km^2	square kilometers	0.386	square miles	mi^2
VOLUME				
mL	milliliters	0.034	fluid ounces	fl oz
L	liters	0.264	gallons	gal
m^3	cubic meters	35.314	cubic feet	ft^3
m^3	cubic meters	1.307	cubic yards	yd^3
MASS				
g	grams	0.035	ounces	oz
kg	kilograms	2.202	pounds	lb
Mg (or "t")	megagrams (or "metric ton")	1.103	short tons (2000 lb)	T
TEMPERATURE (exact degrees)				
^oC	Celsius	1.8C+32	Fahrenheit	^oF
FORCE and PRESSURE or STRESS				
N	Newtons	0.225	poundforce	lbf
kPa	Kilopascals	0.145	poundforce per square inch	lbf/in^2

*SI is the symbol for the International System of Units. Appropriate rounding should be made to comply with Section 4 of ASTM E380.
(Revised March 2003)

ACKNOWLEDGMENTS

This work was funded by the National Highway Traffic Safety Administration (NHTSA) under cooperative agreement DTNH22-10-H-00288 with the University of Michigan. The opinions expressed herein are those of the authors and do not necessarily represent those of NHTSA. The authors acknowledge the valuable contributions of Laura Malik, Jamie Moore, and Brian Eby to this study. We also thank the many students who processed scan data.

CONTENTS

ABSTRACT

A laboratory study was conducted to develop statistical models of posture and body shape for children. Whole-body laser-scan data were obtained from 150 boys and girls ages 4 to 12 in a wide range of postures. Standard anthropometric measures were taken and additional three-dimensional body landmark locations were measured with the children sitting on a vehicle seat with and without a belt-positioning booster. A statistical analysis of the body scan data was conducted to develop models of standing and seated body shapes. The models are parameterized by stature, body weight, and erect sitting height; torso recline and flexion can be adjusted in the seated model. The seated model outputs were compared with the scanned shapes of the Hybrid-III 6YO and 10YO ATDs. The largest discrepancies were noted in the upper thorax and lap areas. The data and models generated in this project will find a wide range of applications in crash safety, including providing guidance for the development of child dummies, computational models of children, and child restraint systems. UMTRI has made the models available online at http://childshape.org/ and http://childshape.org/seated/.

INTRODUCTION

The size and shape of the current physical and computational surrogates of children used for restraint system assessments are based largely on standard anthropometric dimensions, such as lengths, widths and circumferences, obtained in erect standing or erect seated postures. These scalar data provide valuable information on the overall size of the individual, but do not provide good guidance on shape or posture. In particular, the currently available data do not provide useful information on the shape of the torso in relaxed seated postures typical of children sitting in vehicles.

The most widely cited anthropometric data for U.S. children were gathered by the University of Michigan Transportation Research Institute (UMTRI) in the 1970s (Snyder et al. 1977). These data were used in the development of specifications for the child ATDs in the Hybrid-III family (Mertz et al. 2001). The Hybrid-III ATD development also referenced three-dimensional (3D) body forms created in the early 1970s through artistic interpretation based on traditional data (Reynolds et al. 1976).

Efforts to gather more complete posture and shape data from children have focused on single subjects or individual landmarks. Reed et al. (2001) used foam casting and point digitization to develop a 3D surface specification for a physical surrogate representing a six-year-old (6YO) child. In a series of studies, UMTRI has characterized the seated postures of children by recording the locations of body landmarks quantifying skeletal posture in a wide range of vehicle and laboratory conditions (Reed et al 2005; Reed et al. 2006; Reed et al. 2008; Reed et al. 2009; Reed et al. 2013). These data provide more information than conventional anthropometric data but are not sufficient for generating surrogates with realistic contours.

Advancements in surface measurement technology over the past 20 years have enabled a revolution in anthropometric studies. A large number of large-scale surveys of adult populations have been conducted, including the CAESAR and SizeUSA surveys of adult civilians (Robinette et al. 1999) and military surveys (Gordon et al. 2015). However, no large-scale studies of the body shapes of U.S. children have been conducted until the current work. Advances in the analysis methods suitable for high-resolution surface scan data have been equally important. The current study uses methods developed at UMTRI over the past 15 years that have previously been used to model adult body shape (Reed and Parkinson 2008) as well as the shapes of skeletal components (Reed et al. 2009, Shi et al. 2014, Klein et al. 2015).

The objectives of this study were:

1. Gather a comprehensive database of seated and standing surface anthropometry for children ages 4 to 12 years, and

2. Create statistical models of child body shape, along with landmark and joint center locations, suitable for use in the development of physical and computational surrogates of children for safety applications.

METHODS

Overview of Approach

The study protocol was approved by the University of Michigan Institutional Review Board (IRB) for Health Behavior and Health Sciences (IRB # HUM00054993). Participants were recruited through online advertisements, newspaper advertisements, flyers at child centers and other facilities, and word of mouth. Written informed consent was obtained from the parent or guardian of each participant. The parent or guardian was present during testing and was paid $12 per hour for participating. The participant changed into test clothing and standard anthropometric measures were taken. Body landmark locations were recorded in a laboratory hardseat and on a vehicle seat with and without a belt-positioning booster. The body shape of each participant was measured in up to 21 postures using a whole-body laser scanner and specially constructed seating fixtures. Joint center locations were estimated using the surface landmarks. Surface landmark locations were extracted from surface scan data in software. Custom software and methods were used to fit a uniform template to the body scan data for selected standing and seated postures. Statistical body shape models were developed that predict body shape, surface landmarks, and joint center locations as a function of gender, stature, and body weight for standing and seated postures.

Participants

One hundred and fifty children (77 boys and 73 girls) between the ages of 4 and 12 participated in this study. Figure 1 shows the stature and body weight relative to the targets for the 6YO and 10YO Hybrid-III ATDs (Mertz et al. 2001).

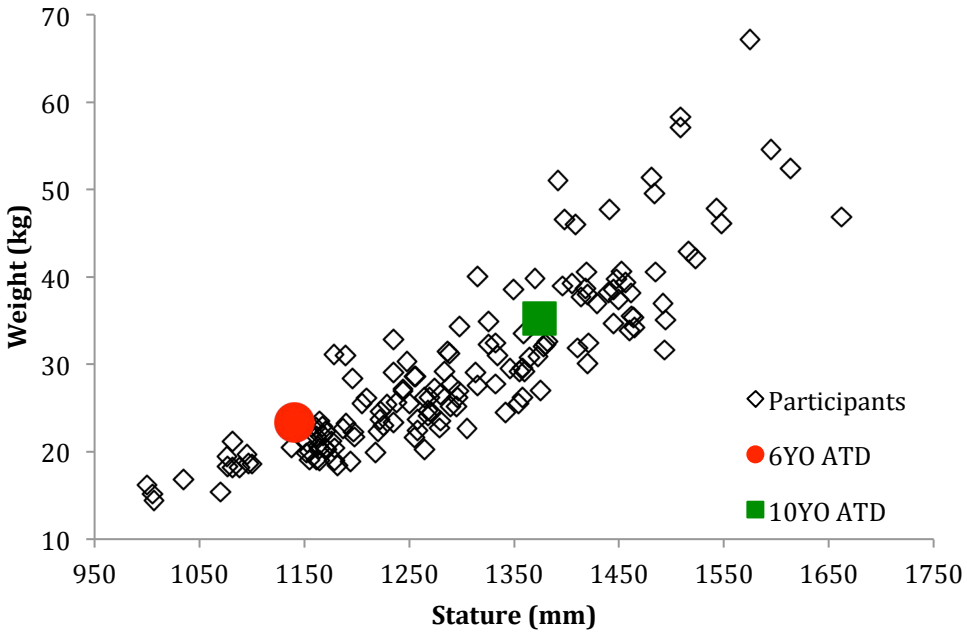

Figure 1. Stature and body weight for participant pool (73 girls and 77 boys) along with manufactured (not target) stature and weight for the 6YO and 10YO Hybrid-III ATDs.

Standard Anthropometry

Standard anthropometric dimensions were obtained using methods and definitions from Gordon et al. (1989). Table 1 lists the information obtained from each participant. Figure 2 shows the measurement of two dimensions. Table 2 lists summary statistics for the participants. Note that the modeling methods do not require this population to be representative of any particular population – it is sufficient that the study sample be broadly distributed.

Table 1
Standard Anthropometric Dimensions

Stature	Head Length	Shoulder Breadth
Body Weight	Head Breadth	Chest Depth (on Scapula)
Erect Sitting Height	Shoulder-Elbow Length	Chest Depth (on Spine)
Eye Height (Sitting)	Elbow-Hand Length	BiASIS Breadth
Acromial Height	Max Hip Breadth	Chest Circumference
Knee Height	Buttock-Knee Length	Waist Circumference
Head Height	Buttock-Popliteal Length	Hip Circumference
	Biacromial Breadth	Upper Thigh Circumference

Figure 2. Examples of investigator measuring head height and stature of a participant

Table 2
Participant Characteristics (N=150)

					Percentiles				
Measurements*	**Mean**	**SD**	**Min**	**Max**	**5th**	**25th**	**50th**	**75th**	**95th**
Age (yr)	8	2	4	12	5	7	8	10	11
Weight (kg)	30	10	14	67	18	22	27	35	49
Body Mass Index (kg/m^2)	17	3	13	27	14	15	16	18	23
Stature	1298	137	1000	1662	1082	1189	1285	1407	1513
Erect Sitting Height	687	58	535	822	588	645	685	729	785
Eye Height (Sitting)	577	56	462	722	484	539	574	616	670
Acromial Height	427	44	326	540	356	396	426	458	500
Knee Height	404	52	288	532	323	364	399	441	485
Head Height	124	82	94	1118	101	112	117	122	131
Head Length	181	9	147	212	165	175	180	186	195
Head Breadth	146	6	130	161	137	141	146	150	155
Shoulder-Elbow Length	268	65	193	963	213	241	264	285	324
Elbow-Hand Length	346	41	257	455	285	313	343	375	416
Max Hip Breadth	251	36	182	363	203	225	247	277	318
Buttock-Knee Length	437	64	140	606	356	390	429	483	537
Buttock-Popliteal Length	367	49	250	484	298	325	363	404	448
Biacromial Breadth	270	32	206	358	219	247	268	286	333
Shoulder Breadth	324	39	250	445	275	293	316	346	393
Chest Depth (on Scapula)	165	24	125	248	135	148	159	179	210
Chest Depth (on Spine)	146	19	112	217	122	132	143	157	180
BiASIS Breadth	170	20	120	229	141	158	168	183	206
Chest Circumference	667	86	493	975	558	600	653	721	821
Waist Circumference	615	94	308	966	501	545	598	667	777
Hip Circumference	689	94	518	990	568	615	676	747	855
Upper Thigh Circumference	412	65	292	593	320	365	406	455	536

* Measurements in mm unless noted

Hardseat

The locations of body surface landmarks were recorded using a FARO Arm coordinate digitizer as the participant sat in a laboratory hardseat constructed to allow access to both anterior and posterior landmarks. Figure 3 shows a participant being measured, and Figure 4 and Table 3 describe the landmarks. These data were used to estimate internal joint center locations using methods described previously (Reed et al. 1999).

Figure 3. Laboratory hardseat used to obtain posterior and anterior body landmarks in same posture.

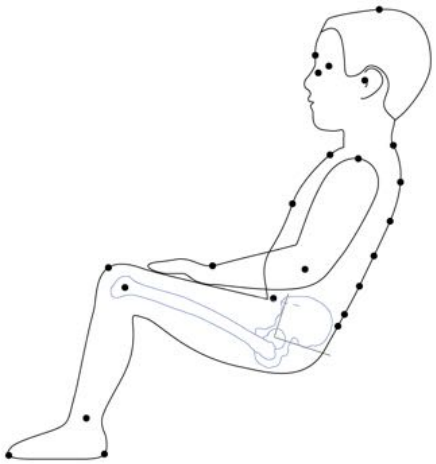

Figure 4. Schematic depiction of body landmarks that were digitized; posterior landmarks were digitized only in the hardseat.

Table 3
Landmarks Digitized In Hardseat

Back of Head	Ulnar Styloid Process (Rt & Lt)	C7
Top of Head	Radial Styloid Process (Rt & Lt)	T4
Tragion (Rt & Lt)	Second Metacarpal, Medial (Rt & Lt)	T8
Ectoorbitale (Rt & Lt)	Fifth Metacarpal, Lateral (Rt & Lt)	T12
Infraorbitale at Pupil Center (Rt & Lt)	Femoral Condyle, Lateral (Rt & Lt)	L1
Glabella	Femoral Condyle,Medial (Rt & Lt)	L2
Suprasternale	Fibula Head, Lateral (Rt & Lt)	L3
Substernale	Tibia, Medial (Rt & Lt)	L4
Anterior Superior Iliac Spine (Rt & Lt)	Suprapatella (Rt & Lt)	L5
Posterior Superior Iliac Spine (Rt & Lt)	Infrapatella (Rt & Lt)	
Clavicle, Medial (Rt & Lt)	Malleolus (Rt & Lt)	
Clavicle, Lateral (Rt & Lt)	Pternion (Rt & Lt)	
Acromion (Rt & Lt)	Acropodion (Rt & Lt)	
Humeral Epicondyle, Lateral (Rt & Lt)	Fifth Metatarsal Phalange, Lateral (Rt & Lt)	
Humeral Epicondyle, Media (Rt & Lt)	First Metatarsal Phalange, Medial (Rt & Lt)	

Table 4
Markers Digitized In Hardseat

Tracking Markers	**Markers on Landmarks**	
3 Upper Arm (Rt & Lt)	Clavicle, Medial (Rt & Lt)	Suprasternale
3 Torso (Rt, Lt & Centerline)	Clavicle, Lateral (Rt & Lt)	Substernale
2 Upper Leg (Rt & Lt)	Humeral Epicondyle, Lateral (Rt & Lt)	Acromion (Rt & Lt)
2 Lower Leg (Rt & Lt)	Humeral Epicondyle, Media (Rt & Lt)	C7
	Ulnar Styloid Process (Rt & Lt)	T4
	Radial Styloid Process (Rt & Lt)	T8
	Top of Wrist	T12
	Bottom of Wrist	L1
	Femoral Condyle, Lateral (Rt & Lt)	L2
	Femoral Condyle, Medial (Rt & Lt)	L3
	Fibula, Lateral (Rt & Lt)	L4
	Malleolus, Lateral (Rt & Lt)	L5
	Medial, Lateral (Rt & Lt)	

Vehicle Mockup

Participant posture and safety belt fit were also measured in the reconfigurable rear seat mockup that was used in previous studies of child posture and belt fit (Reed et al. 2013). Testing was conducted in the right-most outboard seating position. The side bolster on the seat back was removed so that the shoulder belt would have minimal interaction with

seat. The seats were mounted high enough from the floor that none of the children were able to touch the floor while sitting all the way back on the seat, reproducing the typical situation for children in rear vehicle seats. The H-point location, seat back angles, and seat cushion angles were measured using the procedures in SAE J826 (SAE, 2004). The back angle (SAE A40) was set to 23 degrees and the cushion angle (SAE A27) was set to 14.5 degrees. The seat cushion length was set to 471 mm, the mean value for second row seats measured in a previous study (Huang and Reed 2006).

Figures 5 and 6 show the mockup. Participants were measured sitting directly on the seat and sitting on a backless Graco TurboBooster. This booster was chosen because it had been used in several previous studies of child posture, providing a linkage between the current study and those datasets. Table 5 lists the belt anchorage locations used in the mockup and Table 6 lists landmarks measured in each condition.

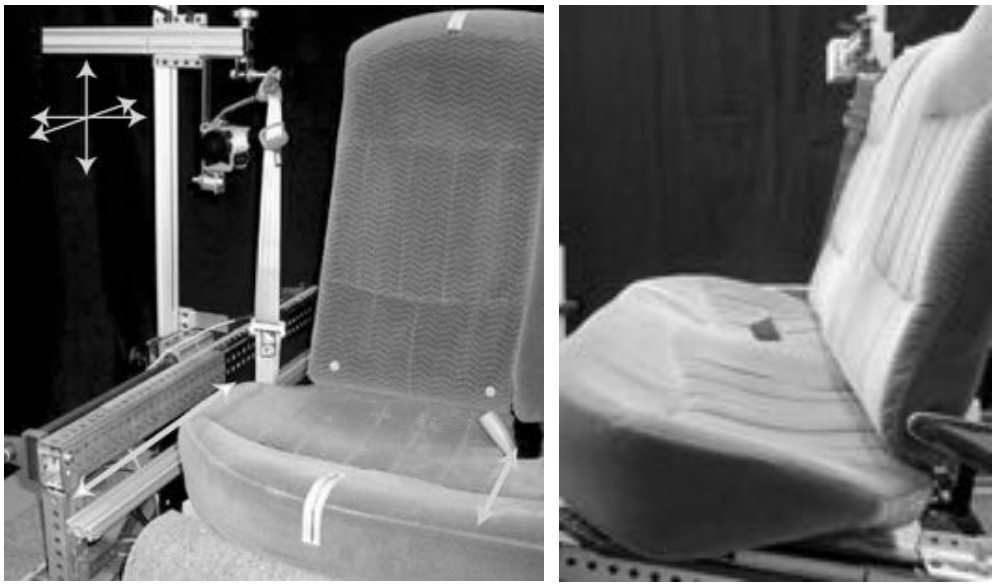

Figure 5. Reconfigurable rear seat and belt.

Figure 6. Investigator recording child posture and belt fit with the child seated on a booster (left) and directly on the vehicle seat (right)

Table 5
Anchorage Locations in Vehicle Mockup Relative to J826 H-Point

Anchorage	XZ Angle (deg)	YZ Angle (deg)	X (mm)	Y (mm)	Z (mm)
Upper Anchor	35	25	399	263	566
Lower Inboard Anchor	51.5		85	200	-104
Lower Outboard Anchor	51.5		112	330	-141

Table 6
Points Digitized in Vehicle Mockup

Back of Head	C7
Top of Head	Anterior Superior Iliac Spine (Rt & Lt)
Tragion (Rt)	Femoral Condyle, Lateral (Rt)
Ectoorbitale (Rt)	Femoral Condyle,Medial (Rt)
Infraorbitale at Pupil Center (Rt)	Suprapatella (Rt)
Glabella	Infrapatella (Rt)
Suprasternale	Malleolus (Rt)
Substernale	Pternion (Rt)
Acromion (Rt & Lt)	Acropodion (Rt)
Clavicle, Medial (Rt)	Fifth Metatarsal Phalange, Lateral (Rt)
Clavicle, Lateral (Rt)	Anterior Superior Iliac Spine (Rt)
Humeral Epicondyle, Lateral (Rt)	
Ulnar Styloid Procsses (Rt)	

Whole-Body Scanning

Body surface contours were recorded using a VITUS XXL whole-body surface scanner and ScanWorX software (Human Solutions). The scanner uses red-light, eye-safe lasers mounted on four towers arranged in a square to project a horizontal line on the subject. Cameras mounted above and below the lasers in each tower record images of the laser line as the heads travel synchronously from top to bottom. Scanning the entire volume requires 12 seconds. The ScanWorX software converts the camera images to range data and then to 3D coordinate data. Approximately 500,000 surface data points are recorded with each scan. The system records grayscale information for each datapoint, enabling visual identification of surface features. This capability was exploited by placing optical markers on body landmarks of interest to enable their 3D locations to be obtained during scan data processing.

Figure 7 shows the process of palpating a landmark and applying a mark. The marks were created by a non-toxic, square ink stamp into which was placed a high-contrast white paint dot. This combination was developed to provide good contrast on a wide range of skin tones. A particular corner of the marker was defined as the location to be picked in the scan data. Figure 8 shows several markers in the grayscale scan image. Table 7 lists the markers and landmarks digitized on the scans. Appendix A provides complete detail on the marker definitions and locations. Specially designed fixtures were constructed to support the participants in the scanner in the desired postures while minimally obstructing the scanner. Figures 11 and 12 show some of the fixtures, including a surrogate booster designed to replicate the seat surface shape of a typical belt-positioning booster. In one condition, participants were scanned in a half-seat to provide access to one undeformed buttock. Figure 13 shows a participant in this condition. Data from a hand-held FARO laser scanner were merged with data from the VITUS data for this and several other conditions.

Up to 21 standing and seated postures were scanned with each participant. Table 8 lists the postures and provides details regarding the fixture configurations and target body segment angles. Figures 14 through 19 show the range of postures, grouped by posture category. The postures were chosen to demonstrate a large range of spine, upper-extremity, and lower-extremity postures typical of standing and seated conditions. In some of the seated postures, a handheld scanner was used to record the lap area, which was shadowed from the VITUS laser scanner. Figure 20 shows this scanning process and Figure 21 shows the merger of data from the two scanners to obtain a complete surface representation.

Figure 7. Applying markers to the skin of a participant.

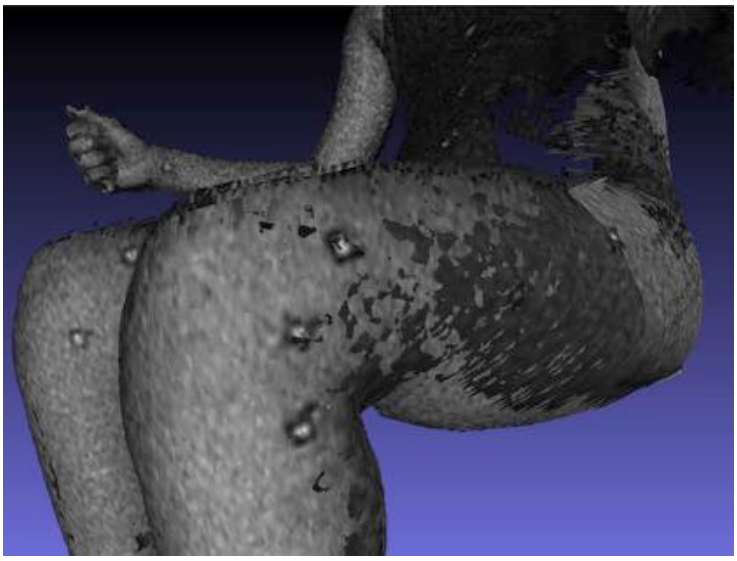

Figure 8. Landmark markers as viewed on the grayscale scan data.

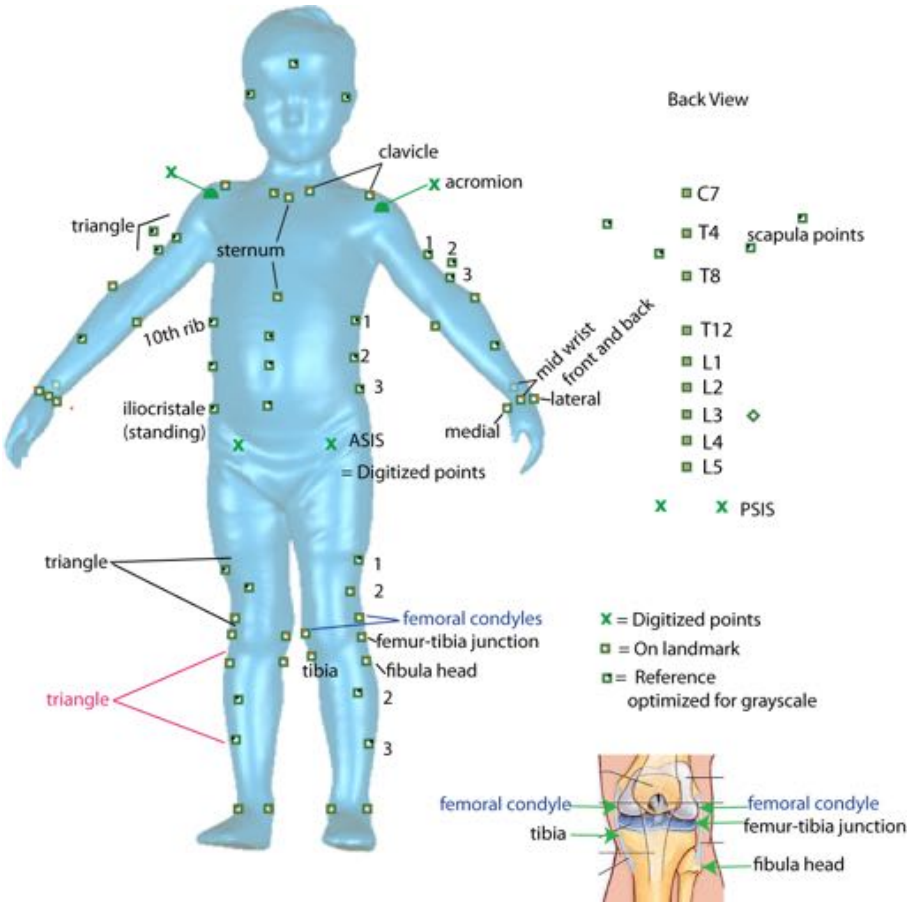

Figure 9. Marker locations (squares) and points digitized with Faro Arm (indicated by Xs).

Table 7
Points Digitized on Scans

Name	No Marker	As Reference	On Landmark	Name	No Marker	As Reference	On Landmark
Ectoorbitale (Rt & Lt)	x			2 Upper Leg (Rt & Lt)		x	
Infraorbitale at Pupil Center (Rt & Lt)	x			2 Lower Leg (Rt & Lt)		x	
3 Head (Rt & Lt)	x			Femoral Condyle, Lateral (Rt)		x	x
Tragion (Rt & Lt)	x			Femoral Condyle,Medial (Rt)		x	x
Back of Head		x		Fibula Head, Lateral (Rt & Lt)		x	x
Top of Head	x			Femur-Tibia Junction (Rt & Lt)			x
Suprasternale			x	Tibia, Medial-Proximal (Rt & Lt)			
Suprasternale			x	Malleolus, Lateral (Rt & Lt)			x
Acromion (Rt & Lt)			x	Malleolus, Medial (Rt & Lt)			x
Clavicle, Medial (Rt)			x	Pternion (Rt & Lt)	x		
Clavicle, Lateral (Rt)			x	Acropodion (Rt & Lt)	x		
3 Upper Arm (Rt & Lt)		x		5th Metatarsal Phalange, Lateral (Rt & Lt)	x		
Humeral Epicondyle, Lateral (Rt & Lt)			x	1st Metatarsal Phalange, Medial (Rt & Lt)	x		
Humeral Epicondyle, Media (Rt & Lt)			x	C7			x
1 Lower Arm (Rt & Lt)		x		T4			x
Ulnar Styloid Process (Rt & Lt)			x	T8			x
Radial Styloid Process (Rt & Lt)			x	T12			x
Top of Wrist		x	x	L1			x
Bottom of Wrist		x	x	L2			x
Second Metacarpal, Medial (Rt & Lt)	x			L3			x
Fifth Metacarpal, Lateral (Rt & Lt)	x			L4			x
3 Torso Midline		x		L5			x
10th Rib, Lateral (Rt & Lt)		x	x	Axilla, Anterior (Rt & Lt)	x		
1 Mid Torso Line (Rt & Lt)		x		Axilla, Posterior (Rt & Lt)	x		
Iliocristale (Rt & Lt)		x	x	Thigh-Abdominal Junct, Lateral (Rt & Lt)	x		
FootToe1Lt	x			Thigh-Abdominal Junct., Medial (Rt & Lt)	x		
FootHeelRt	x			Scapula, Lateral (Rt & Lt)		x	x
FootHeelLt	x			Scapula, Medial (Rt & Lt)		x	x

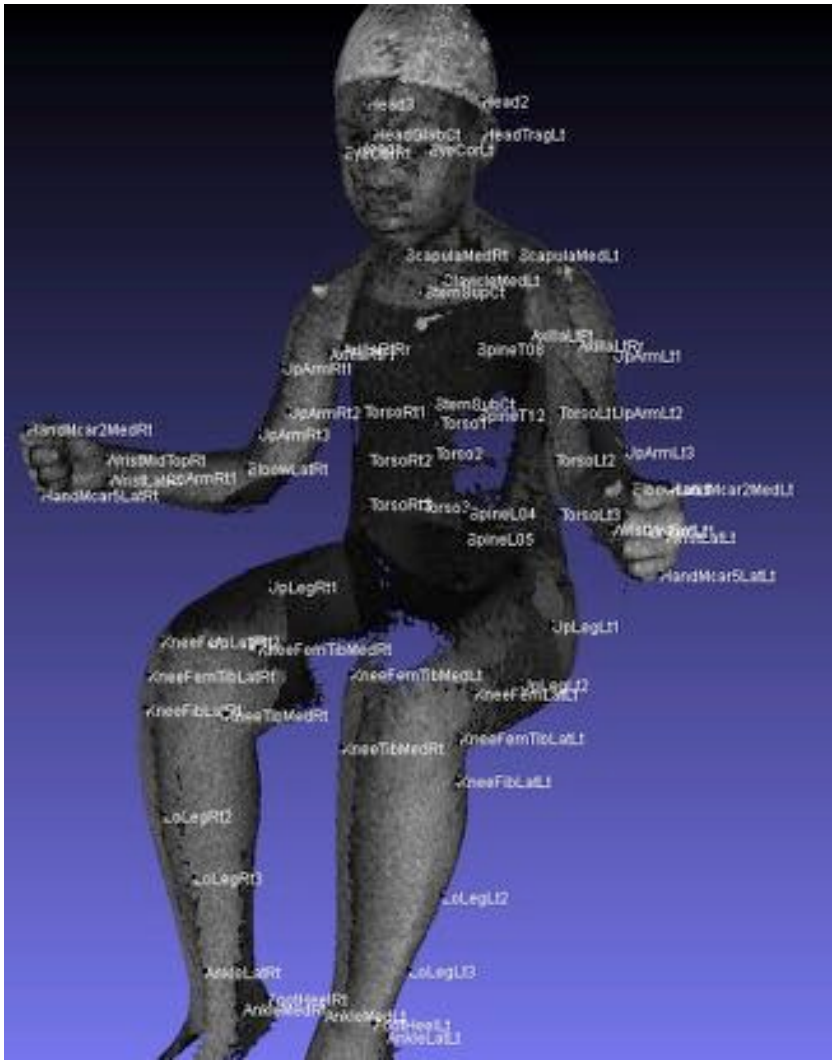

Figure 10. Markers and landmarks digitized in grayscale image of scan.

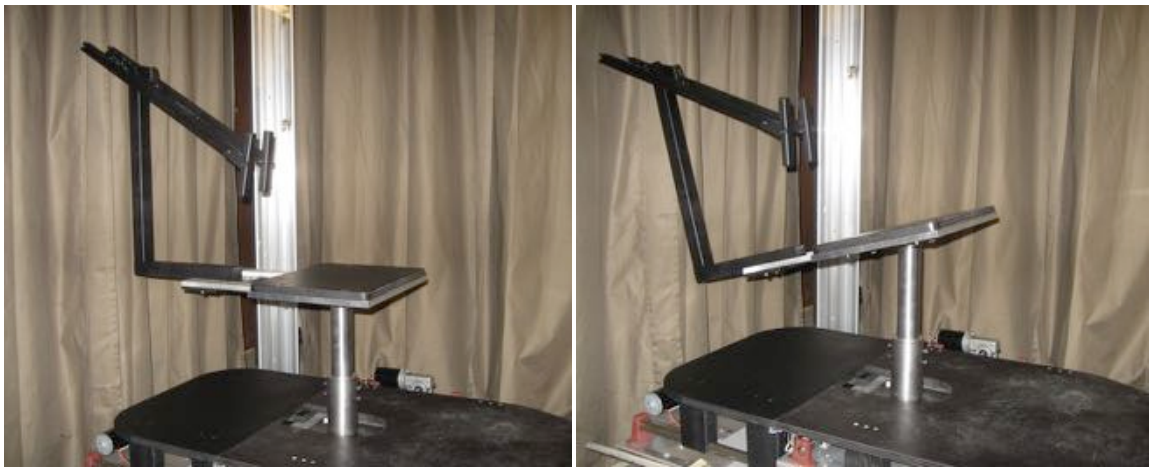

Figure 11. Upright (left) and reclined (right)

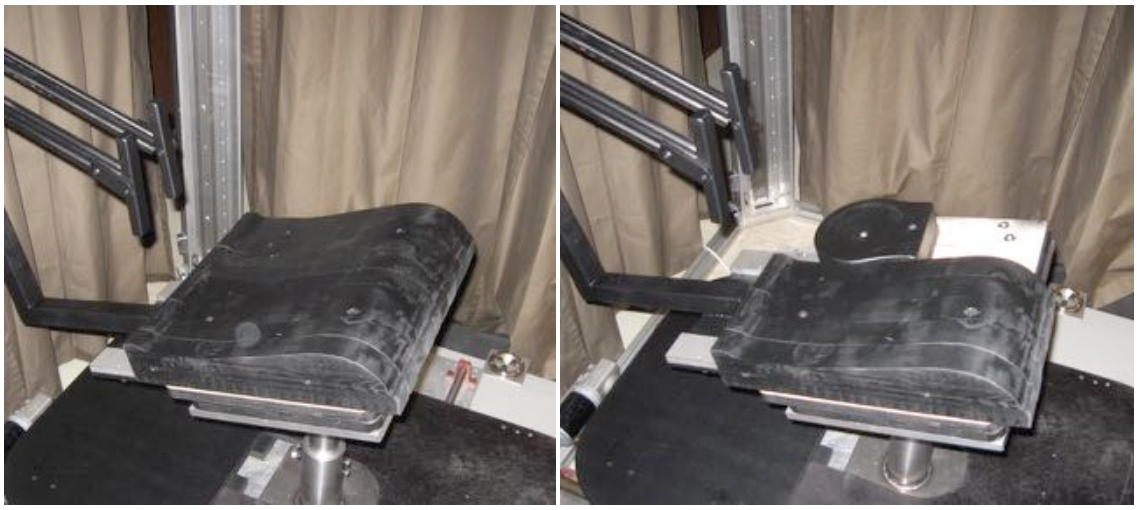

Figure 12. Booster (left) and half booster seat (right)

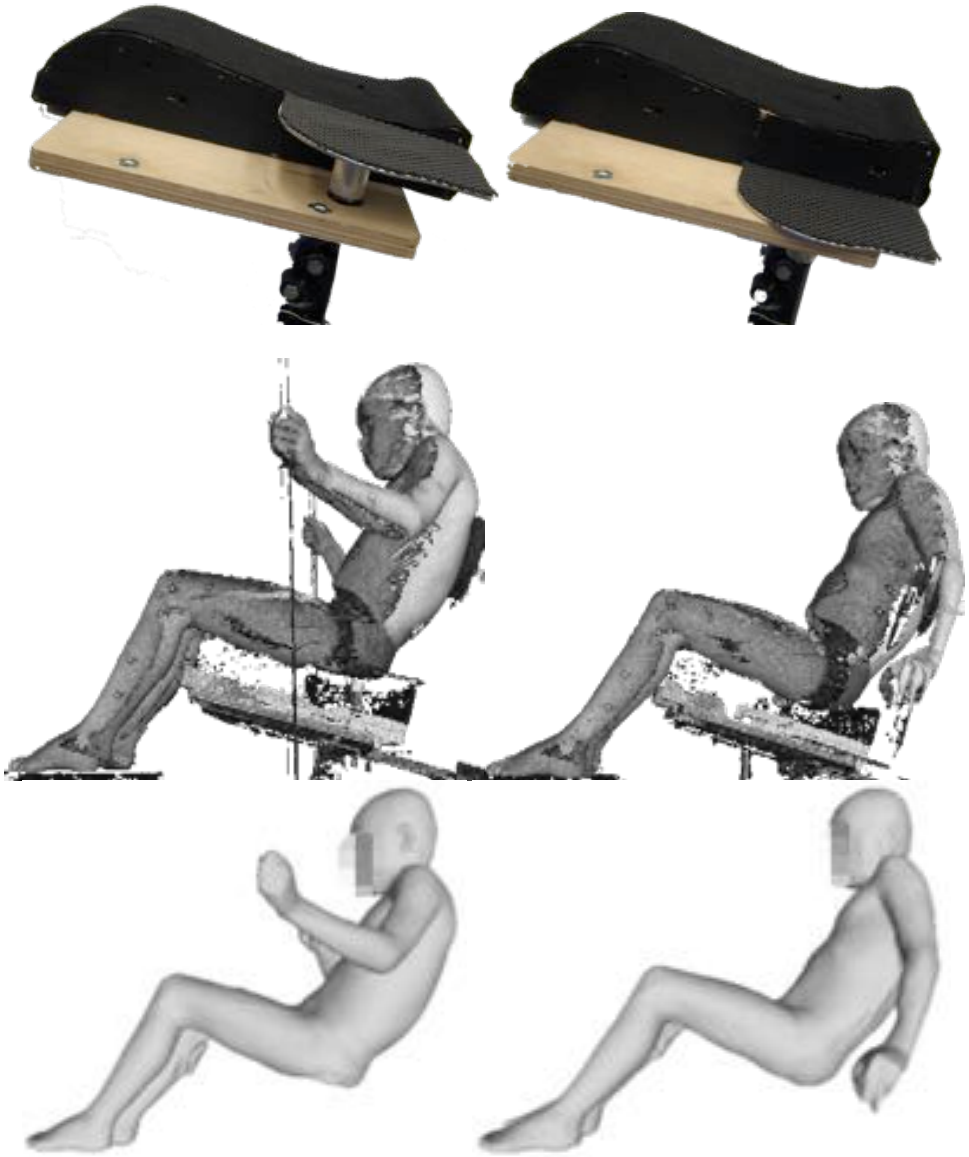

Figure 13. Booster and booster half seat (above), grayscale scans (middle) and meshes with full-body scan and hand-held scanner data merged.

Table 8
Scanned Postures

Scan	Name	Seat Pan	Seat Back	Hip Position	Feet	Spine Position	Arm Position	Hand-held Scan	Faro Dig. Pts
Reclined	R1	14.5°	23°	Fit Seat		Erect	Handle	Yes	Yes
	R2					Slumped a little		Yes	Yes
	R3					Slumped more		Yes	Yes
	R4					Maximal slump		Yes	Yes
Booster-Type Seat	1			Booster		Booster seat posture		Yes	Yes
Booster- Half of Seat	1	Half	Half	Booster				Yes	Yes
Sitting Lap	L1	Level	None	75° Flexion		Erect		Yes	Yes
Sitting ISO	L2			Flex 90°			90˚ Elbow Flexion	Yes	Yes
Shoulder Flexion 90˚	A1						90° Flexion	No	No
Shoulder Flexion Maximum	A2						Maximum Flexion		
Shoulder Abduction 90˚	A3						90° Abduction		
Shoulder Abduction Maximum	A4						Maximum Abduction		
Shoulder Extension Maximum	A5						Extension		
Spine Flexion Minimum	V1					Flex min	Handle		
Spine Flexion Maximum	V2					Flex mid	Handle		
Spine Flexion Mid-range	V3					Flex max	Handle		
Spine Extension Maximum	V4					Ext max	Handle		
Standing Natural	T1	None		Zero	10 cm apart	Natural	Natural		Yes
Standing Arms Abducted	T2						30° Abduction		Yes
Standing Erect	T3					Erect			Yes
Standing T-pose	T4				30 cm apart	Natural	90° Abduction		Yes

Handle = Arms raised away from body while keeping shoulders in a neutral position

Table 9
Description of Postures

Posture	Purpose and Description
Recline 1 - 4	A series of postures in which the subject goes from a very erect posture to a very slumped posture, while keeping the knee angle constant. The seat is set with a 23˚ back angle and 14.5˚ cushion angle. The seatback moves rearward to increase the slump. The hips stay forward on the seat so that the bottoms of the thighs and backs of the calves are scanned well. Seat surface should not cut into the back of the thighs. The arms are forward so that the sides of the torso scan well – but the shoulders are still in a resting position (as if arms were hanging by the side of the subject). Elbows and shoulders are relaxed with the subject's hands on the handles supporting the weight of the arm.
Sitting Lap	An erect posture on a level seat in which the tops of the thighs are visible in the full body scanner
Sitting ISO	A posture from the ISO standard for scanning
Booster	A posture very similar to that of a child in a booster seat (backless Turbo Booster). The fore-aft distance between the tragion and ASIS of the subject in this posture are set using the values collected on the subject while sitting on the booster in the vehicle seat (Grand Am buck). The backs of the calves should not be touching the front of the booster seat.
Booster Half Seat	A posture in which half of the subject's body is fully scanned – including the back and under the buttocks
Shoulder Flexion, Extension and Abduction	A series of arm positions used to get surfaces of the shoulder, neck and torso
Spine Flexion Min, Mid, Max	A series of postures in which the back goes from natural sitting to as much like the letter "C" as possible. In maximum flexion the chin is on the chest.
Spine Extension, Max	Entire spine – neck to lower back arched as much as can safely be done
Standing Natural	Natural, yet symmetrical, standing posture to get a good scan of arms hanging at sides
Standing Arms Abducted	Similar to Natural but with arms away from body to get a good scan of torso
Standing Erect	Similar to Standing Arms Abducted, but with spine erect
Standing T-pose	Arms abducted 90˚ and legs wide used to get under arm and between leg surfaces

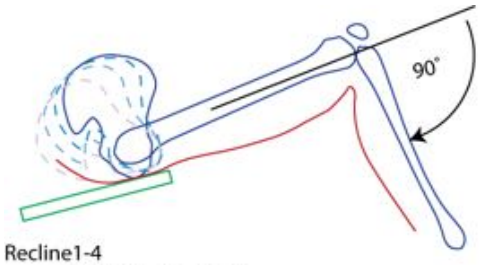

Recline1-4

Upright - Reclined
Knee flexion = 90°
Knee and ankle spacing controlled
Feet probably on blocks
Minimal subject <-> seat contact:
Hips far forward on seat
Back of thighs off of seat surface (may need to raise knees)

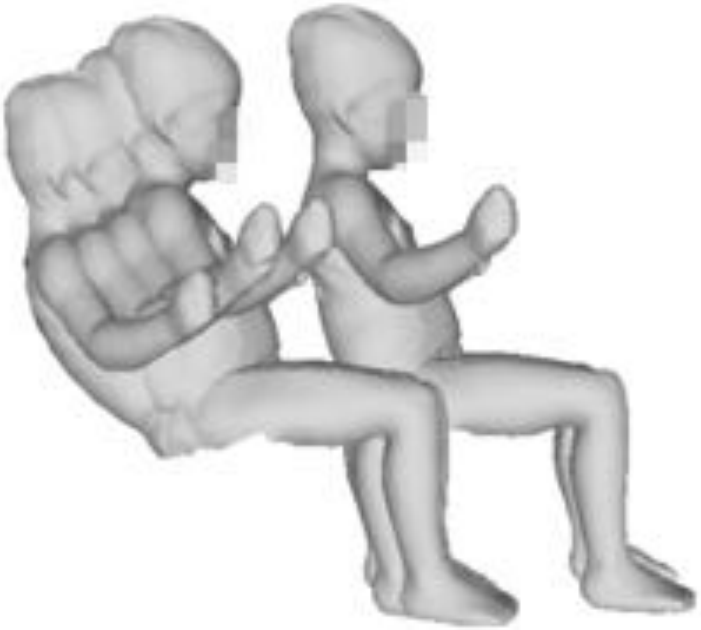

Figure 14. Recline postures

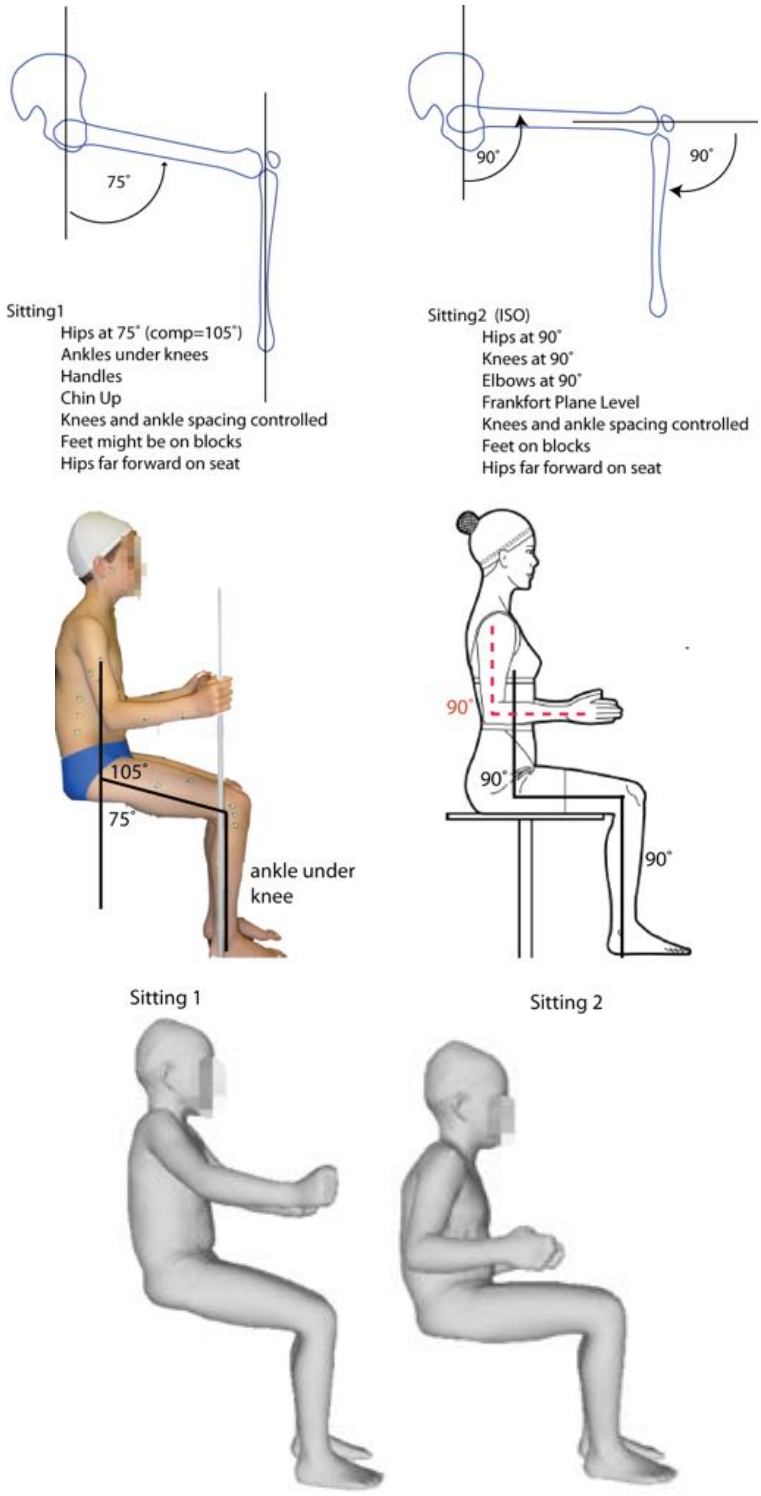

Figure 15. Lap and ISO postures

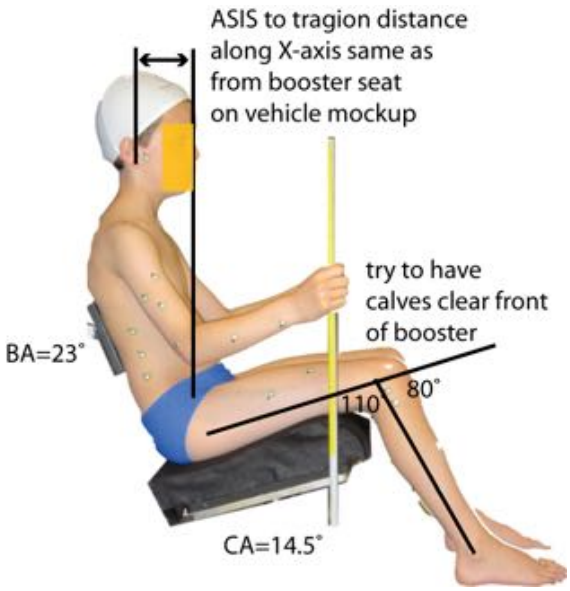

Figure 16. Booster seat posture

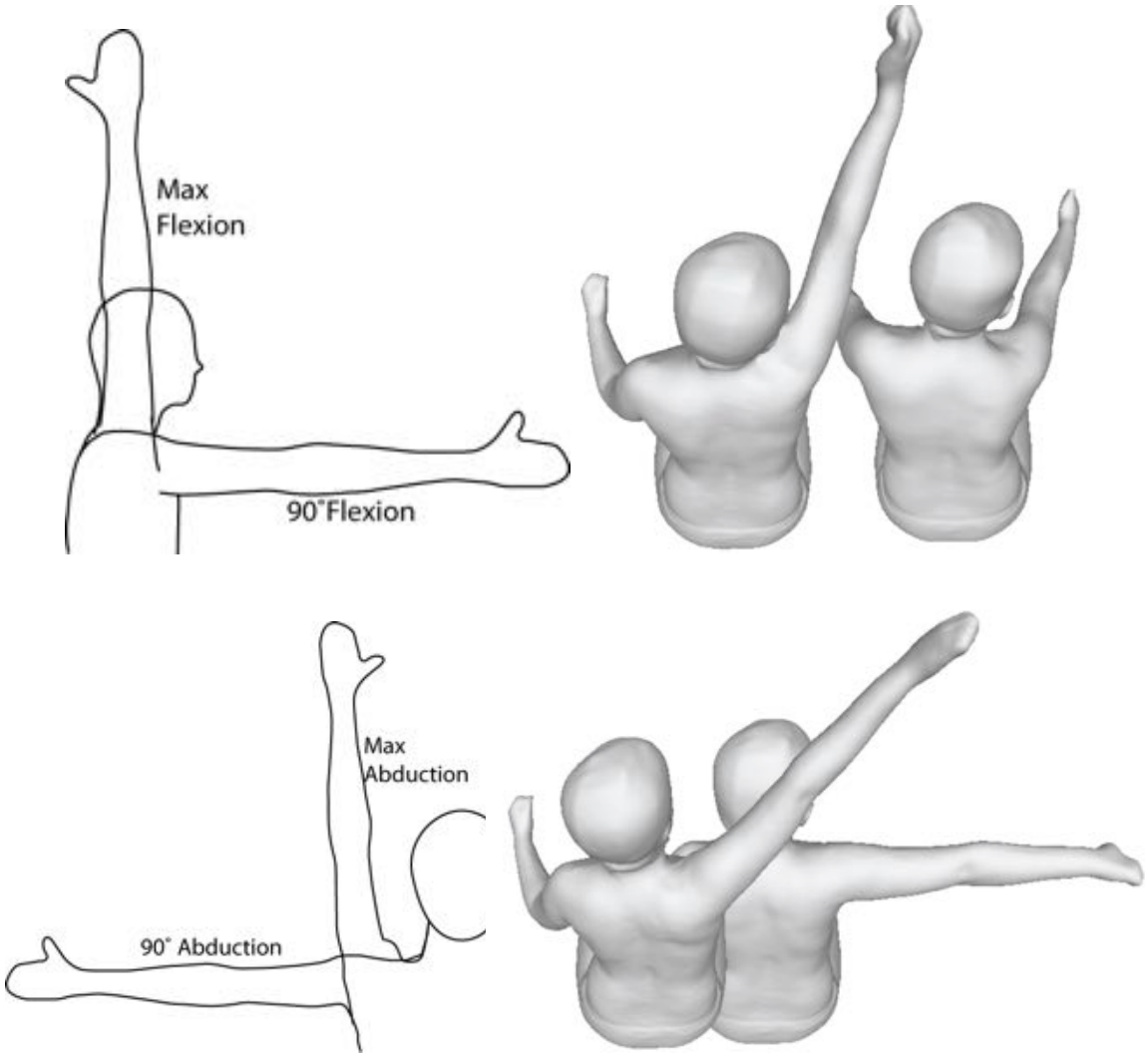

Figure 17a. Shoulder range-of-motion scans.

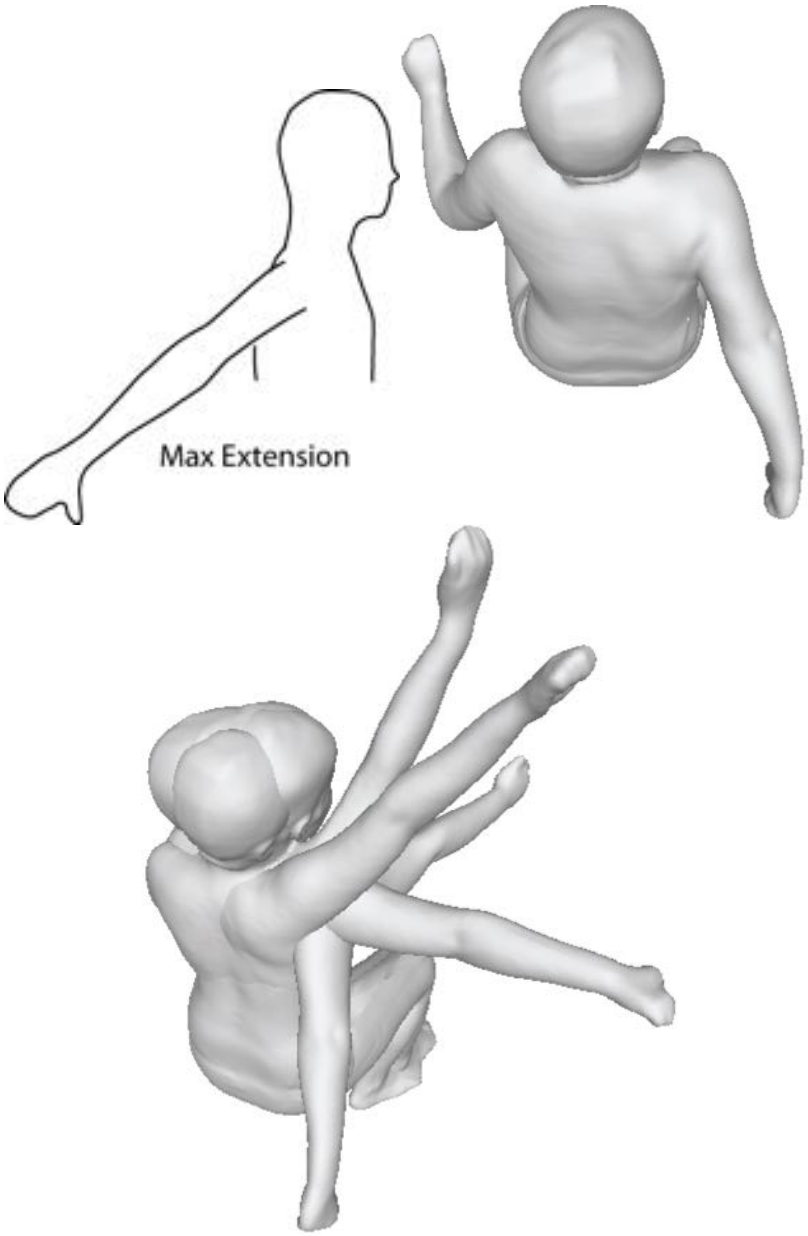

Figure 17b. Shoulder range of motion

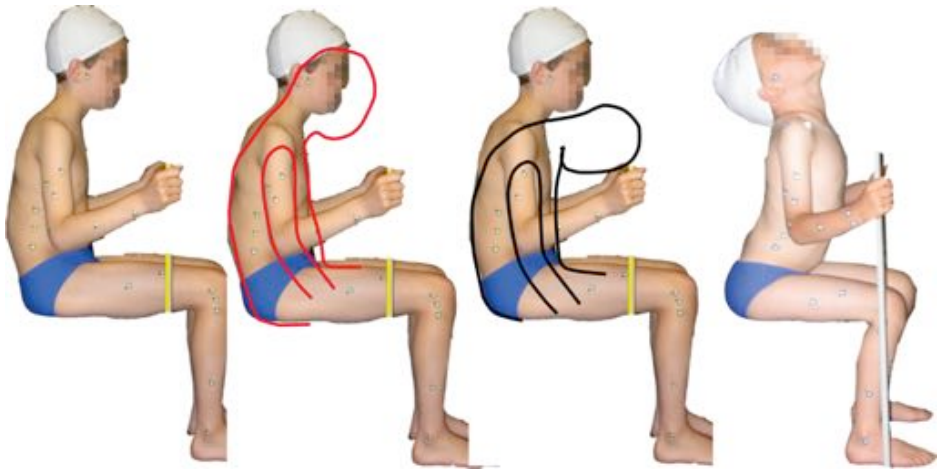

Figure 18a. Spine range of motion.

Figure 18b. Spine range-of-motion.

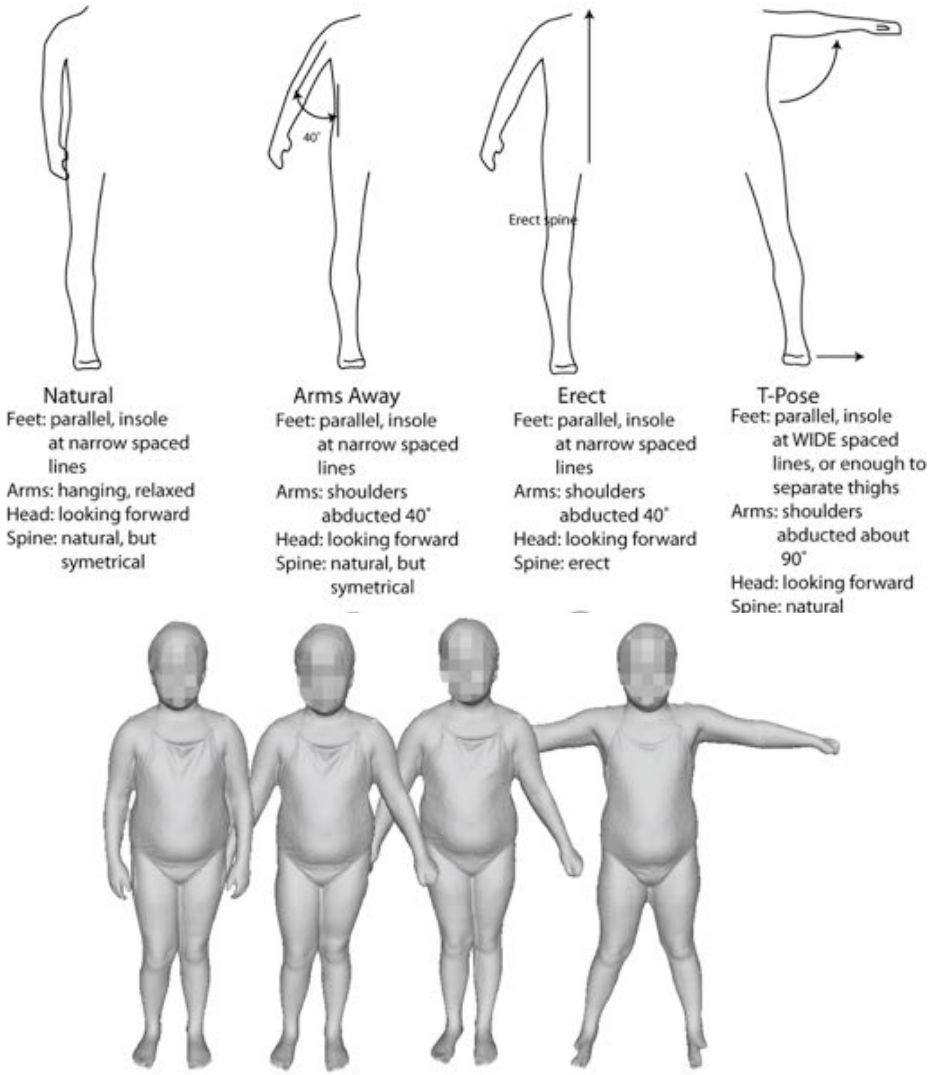

Figure 19. Standing postures.

Figure 20. Using the FARO Arm to digitize landmarks in the scanner.

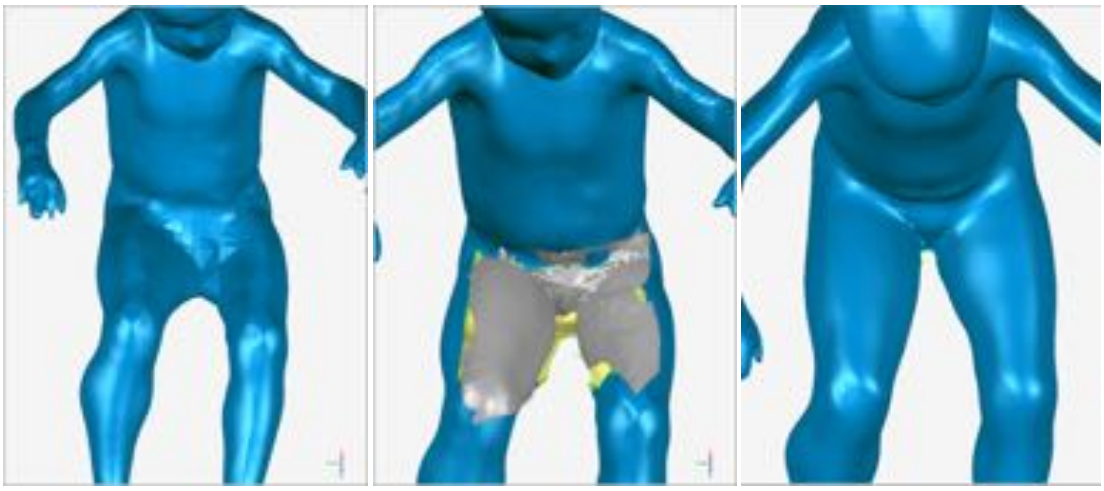

Figure 21. Avatar from full-body scanner (left), process of merging with mesh from hand-held scanner, and merged scan (right).

Scan Summary

Table 10 lists the number of scans processed for each of the scan postures. Not all scans were available for all participants due to problems with the scan quality in some cases. At least 125 scans were obtained for each posture.

Table 10
Scan Summary

Scan	Code	Count	Example	Scan	Code	Count	Example
Recline 1	R1	147		Recline 3	R3	146	
Recline 2	R2	146		Recline 4	R4	145	
Booster-Type Seat	1	138		Booster-Half of Seat	1	126	
Sitting Lap	L1	145		Sitting ISO	L2	144	
Shoulder Flexion 90˚	A1	141		Shoulder Abduction 90˚	A3	140	
Shoulder Flexion Maximum	A2	141		Shoulder Abduction Maximum	A4	139	
				Shoulder Extension Maximum	A5	141	
Spine Flexion Minimum	V1	138		Spine Flexion Mid-range	V3	139	
Spine Flexion Maximum	V2	134		Spine Extension Maximum	V4	139	
Standing Natural	T1	146		Standing Erect	T3	146	
Standing Arms Abducted	T2	145		Standing T-pose	T4	146	

Scan Data Analysis — Standing Posture

Template Fitting

For the standing body shape model, scans of the relaxed standing posture (T2) were used. To facilitate statistical analysis, a standardized template mesh was fit to each scan. This template was generated from one of scans that did not have any visual anomalies on the surface, and this was standardized to be "watertight" (no holes) with 30,002 vertices and 60,000 triangular polygons using MeshLab (http://meshlab.sourceforge.net). As described in Figure 22, the template fitting procedure is composed of two morphing steps: initial morphing to match the body pose and orientation based on synthetic landmarks, and fine morphing to fit the template vertices to the corresponding positions on the target data surface.

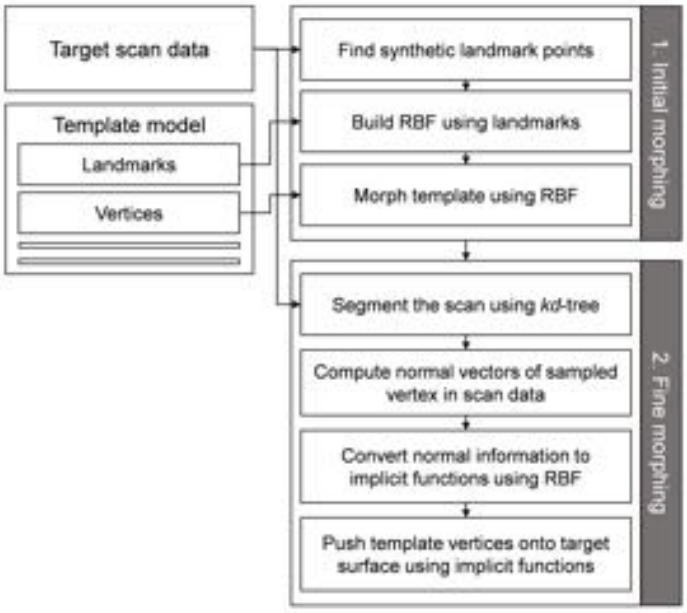

Figure 22. Process to fit a template model to scan data of a specific subject using radial basis function technique.

In the initial morphing step, the 20 synthetic landmarks shown in Figure 23 were used to roughly fit the body shape and the posture of the template mesh to a target scan. The landmarks were automatically found by algorithms based on local geometric features from both of the template and target scan data. An interpolator using a radial basis function (RBF) was then built based on these landmarks to morph the template. In general, an RBF interpolator is a function of the form given by:

$$s(\boldsymbol{x}) = \sum_{i=1}^{N} w_i \varphi(\|\boldsymbol{x} - \boldsymbol{x}_i\|) + p(\boldsymbol{x}), \qquad (1)$$

where $p(\boldsymbol{x}) = a_1+a_2x+a_3y+a_4z$ is a polynomial defined in the null space of the differential operator, the coefficients w_i and a_i are real numbers, $\|\cdot\|$ is the Euclidean norm, and $\varphi(r) = r^2 \log(r)$ is a basis function known as the thin-plate spline. The coefficients of the interpolating function in equation (1) can be found by solving a linear system of equations given by:

$$\begin{pmatrix} \boldsymbol{B} & \boldsymbol{L}_{tpl} \\ \boldsymbol{L}_{tpl}^T & \boldsymbol{O} \end{pmatrix} \begin{pmatrix} \boldsymbol{w} \\ \boldsymbol{a} \end{pmatrix} = \begin{pmatrix} \boldsymbol{L}_{trg} \\ \boldsymbol{O} \end{pmatrix}, \tag{2}$$

where $\boldsymbol{B}_{i,j} = \varphi(\|\boldsymbol{x}_i - \boldsymbol{x}_j\|)$, and $\boldsymbol{O}$ is a zero matrix. $\boldsymbol{L}_{tpl}$ is the matrix of the landmark coordinates of the template with ith row $(1, x_i, y_i, z_i)$, $\boldsymbol{L}_{trg}$ is the matrix of target landmark coordinates. Once the coefficients of the interpolation function $(\boldsymbol{w}, \boldsymbol{a})^T$ are solved from equation (2), all the vertices of the template mesh are moved by equation (1).

Figure 23. Synthetic landmarks over the body shape

For the fine morphing, an implicit-surface function was constructed from the target scan data and the template vertices were moved to the zero surface. The fine fitting process was conducted as follows:

1. Partition the target data into voxels that contain 200 to 300 points sized using *kd*-tree.
2. Within each box:
   a. Assign each surface point a scalar value of zero.
   b. For a subset of the surface points, construct new points that are "inside" and "outside" the surface. Inside and outside points are created by moving along the normal by a margin of 3 mm.
   c. Assign each inside point a value of -1, each outside point a value of 1.

d. Compute an interpolation function (Input: 3D coordinates, output: 1D scalar) using RBF presented in equation (1), such that the function has a value of zero on the surface.

3. For each vertex in the template, move it onto the surface (zero-valued position) using the gradient of the implicit surface function.

Statistical Analysis

A principal component analysis (PCA) was conducted using the methods described in Reed and Parkinson (2008). The coordinates of the mesh vertices are flattened to create a 3×30k geometry vector for each fitted template. The 27 standard anthropometric variable values were appended to each vector along with the 3D coordinates of 135 surface landmarks and estimated joint center locations, resulting in a 135×90447 geometry matrix about 135 subjects. PCA was conducted on this geometry matrix to find the linear projection that reduces dimensions of the matrices while variance in the data is well preserved. The first 200 PC scores were retained from the PCA, representing a statistically significant ($p<0.05$) amount of variance in the geometric data. Following the methods described in Reed and Parkinson (2008), a linear regression analysis was conducted to associate the projected PC scores with subject characteristics such as stature, body mass index (body mass in kilograms divided by stature in meters squared), and the ratio of erect sitting height to stature (SHS) as predictors.

Scan Data Analysis — Seated Postures

For the seated body shape model, data from the unsupported seated posture L1 and the first three recline postures (R1, R2, and R3) were used. A total of 477 scans from 135 children (up to four postures per child) were analyzed. After automated processing to fill holes in the surface mesh, an automated procedure similar to the methods used to fit the standing scans was used to fit a template mesh with 18271 vertices to each scan. PCA was conducted on the mesh data to reduce the dimension and 200 PCs representing more than 99 percent of the variance in mesh coordinates were retained. A regression analysis was conducted to predict body size and shape via PC scores as a function of overall body dimensions (stature, BMI, and the ratio of sitting height to stature) and two measures of torso posture: overall recline and lumbar flexion. Recline was quantified as the orientation of the vector from the mid hip joint center to C7/T1 with respect to vertical. Lumbar flexion was calculated as the pelvis segment orientation minus the thorax segment orientation. A value of zero represents approximately the standing torso posture; values in this seated data set ranged from about 25 to 70 degrees. To account for the expected nonlinearity in posture change with recline angle, the posture angles were represented in the analysis using both sine and cosine of both angles, plus the interaction between each angle and the anthropometric predictors. Thus, the model can account for differences in torso recline behavior as a function of stature or BMI.

Comparisons of Seated Model to ATD Body Shapes

The body shapes of the 6YO and 10YO Hybrid-III ATDs were compared to (1) body shapes of manikins generated with the reference ATD body dimensions and (2) body

shapes of manikins fitted to the ATD body shapes. The ATDs were placed in postures similar to the L2 posture and scanned using the VITUS XXL as shown in Figure 24. The scans were processed using methods similar to those used for the child scans. The seated SBSM was exercised using reference body dimensions for the ATDs from Mertz et al. (2001). Statures of 1168 mm and 1374 mm, BMIs of 15.3 kg/m^2 and 17.2 kg/m^2, and SHS of 0.54 and 0.52 were respectively used for generating 6 YO and 10 YO manikins. A second comparison was conducted by fitting the SBSM to each ATD scan. That is, for each ATD, the set of principal component scores that yielded shape most closely matching the ATD scan was identified by minimizing the distance between the model vertices and the scan data. Errors between the manikin shapes and ATD shapes were measured for each comparison with unsigned distances of the manikin vertices to the closest points of ATD scans.

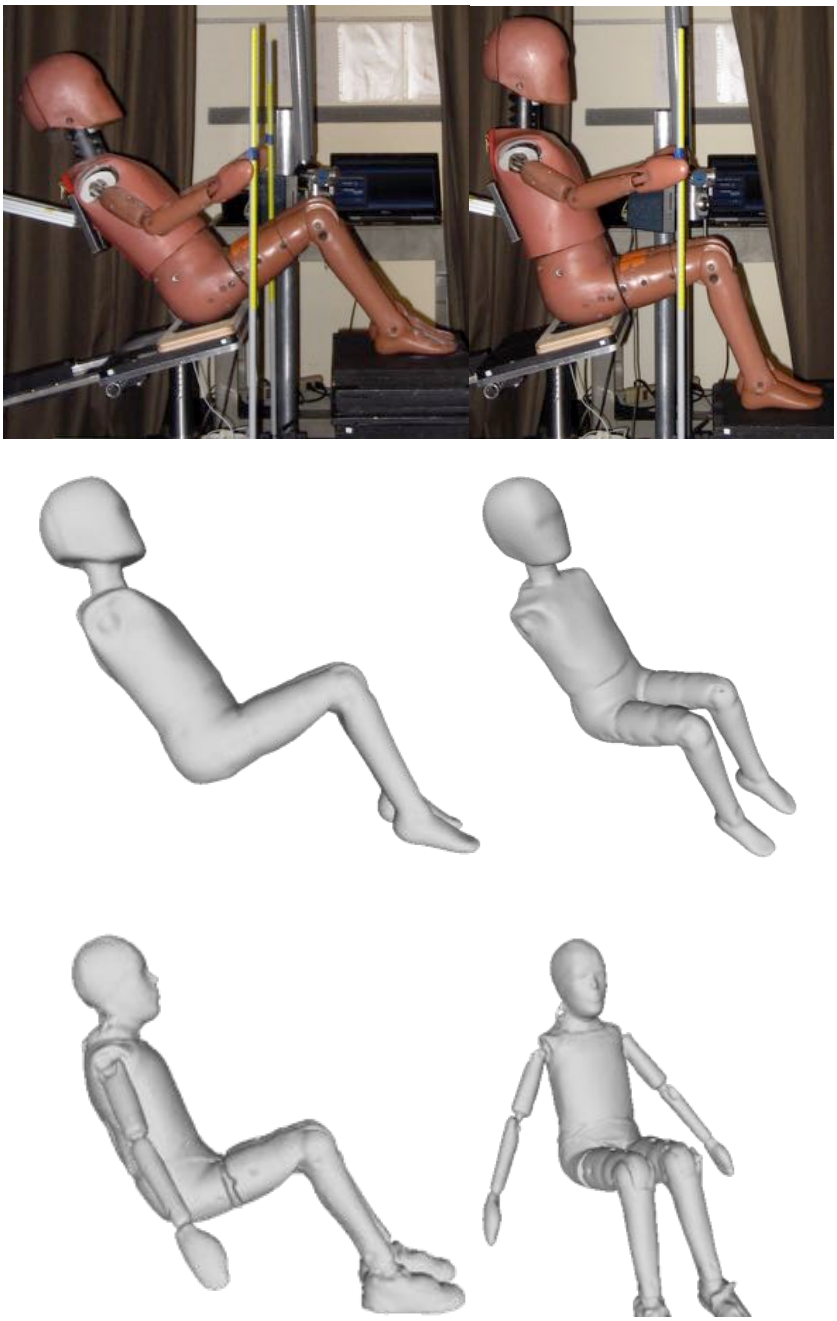

Figure 24. Scanning the 6YO and 10YO Hybrid-III ATDs

RESULTS

Standing Body Shape Model

Figure 25 shows qualitative comparisons between the template mesh (a), results of each template fitting process (b, c), and target scan data (d) of a child.

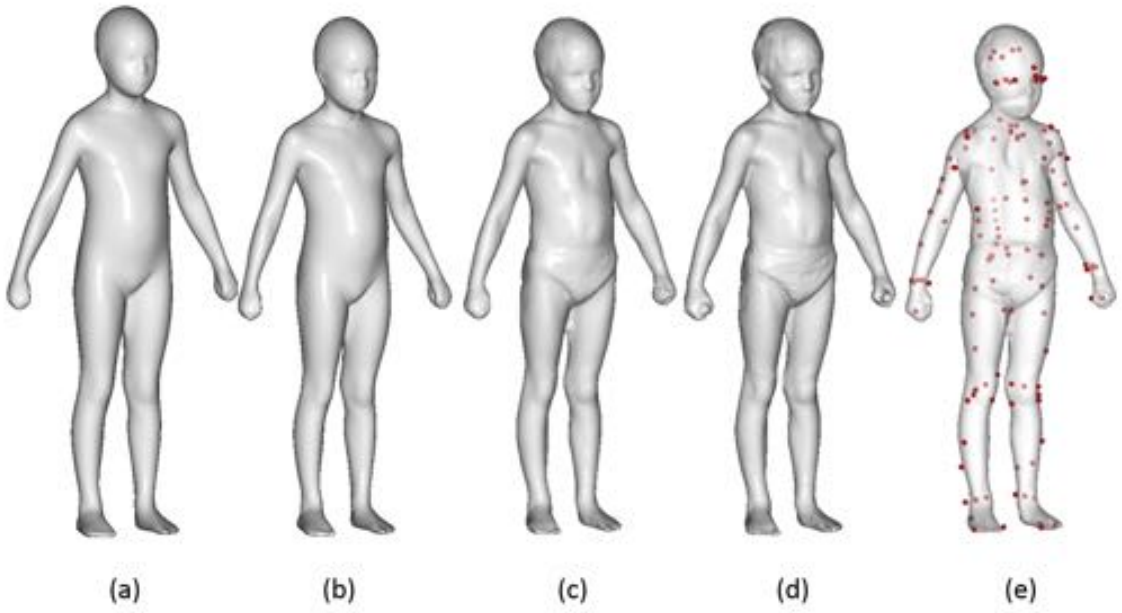

Figure 25. Results of each template fitting step of a person: (a) template mesh, (b) initially morphed template model using RBF, (c) fine-morphed template using implicit-surface-fitting, (d) target laser scan data, and (e) estimated surface landmarks and joints.

Figure 26 illustrates the effects of manipulating stature (100 ~ 160 cm) and BMI (11 ~ 27 kg/m^2) over the range available in the body shape space of the model, while holding SHS at the mean. Figure 27 compares original scans for 10 subjects with the reconstructions using SBSM with 60 PCs. The unsigned distances between the two surfaces at each vertex were coded with the standard heat map corresponding to 0 to 20 mm to assess the error due to limiting the number of PC scores. Mean (±standard deviation) absolute error was 2.2±0.28 mm, and 95^{th} percentile error was 4.51±0.57 mm. In most cases, the maximum errors were found in the back of head, where hair was covered with a swim cap, and in the crotch area, which was shadowed from the scanner.

The explanatory power of the set of predictors such as stature, BMI, and SHS was validated by comparing the scan data with predicted models based on actual anthropometric data of the same subjects. Figure 28 shows the result of this comparison. Errors were coded with a heat map (ranged 0 mm to 50 mm) and were evaluated only for the torso to ignore the effect of limb posture variance.

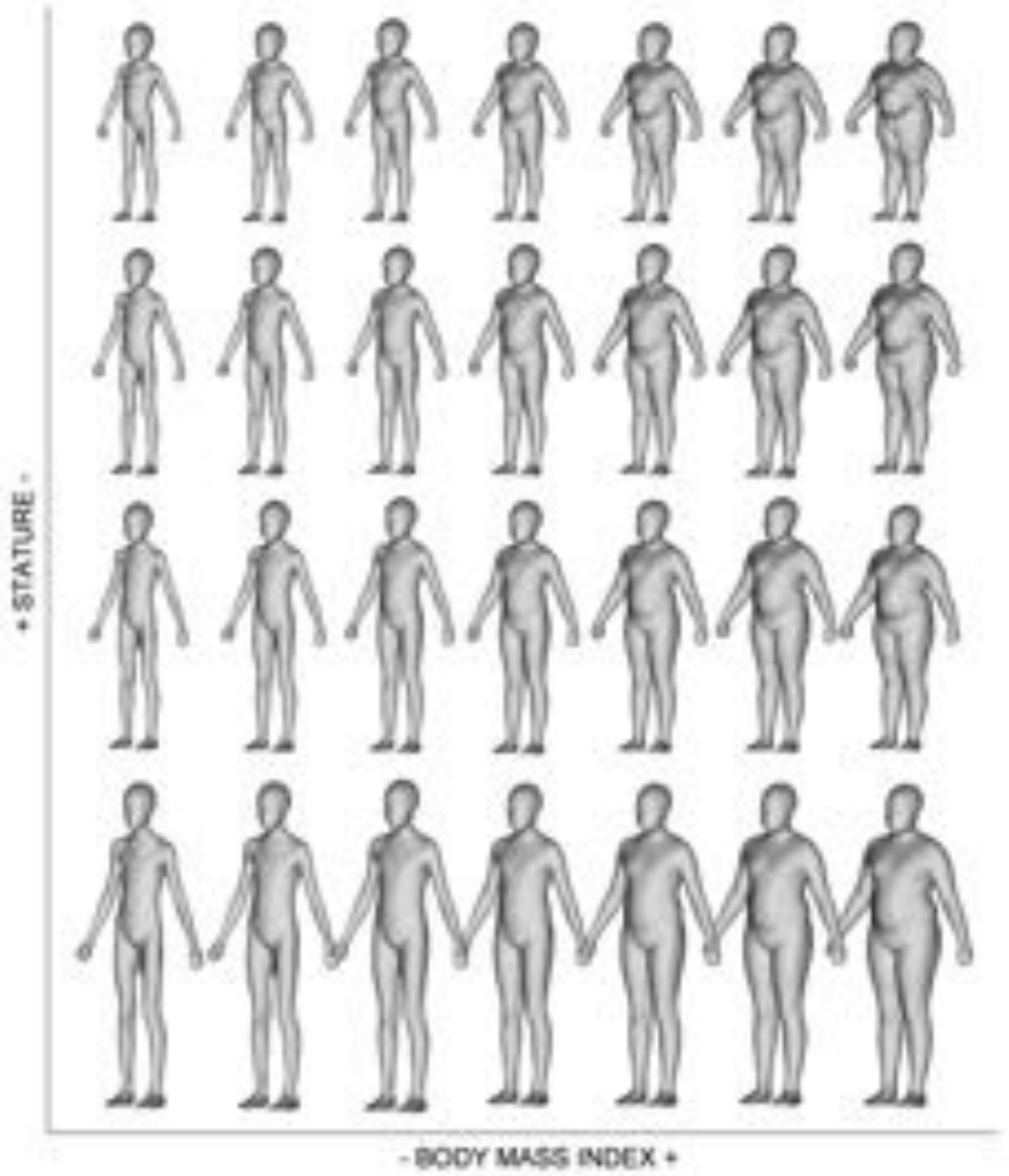

Figure 26. Range of body sizes and shapes. BMI varies along the horizontal axis (11 ~ 27 kg/m^2) and stature effects vary along vertical axis (100 ~ 160 cm).

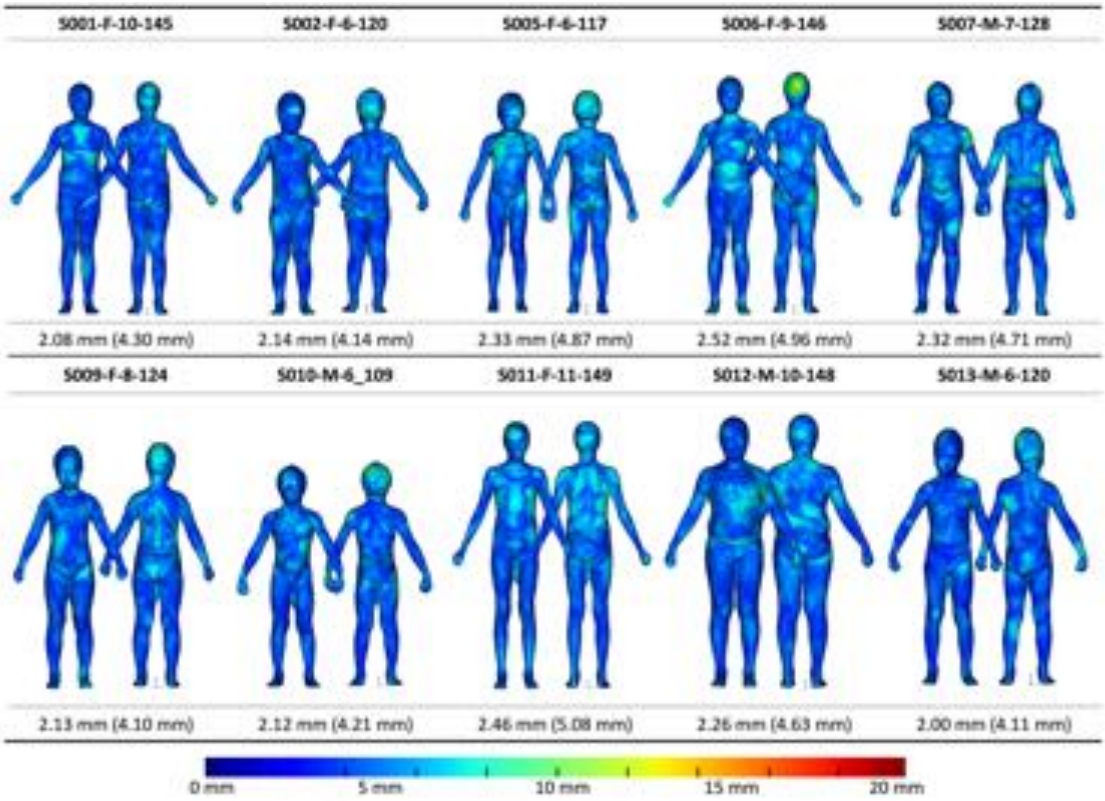

Figure 27. Comparisons between fitted template models and reconstructed data using 60 PC scores of each segment. IDs above each image list gender, age at testing (YO), and height (cm) of the subject. Mean and 95^{th} percentile errors evaluated from the absolute distances between corresponding vertices are stated below each image. Left is front side and right is backside.

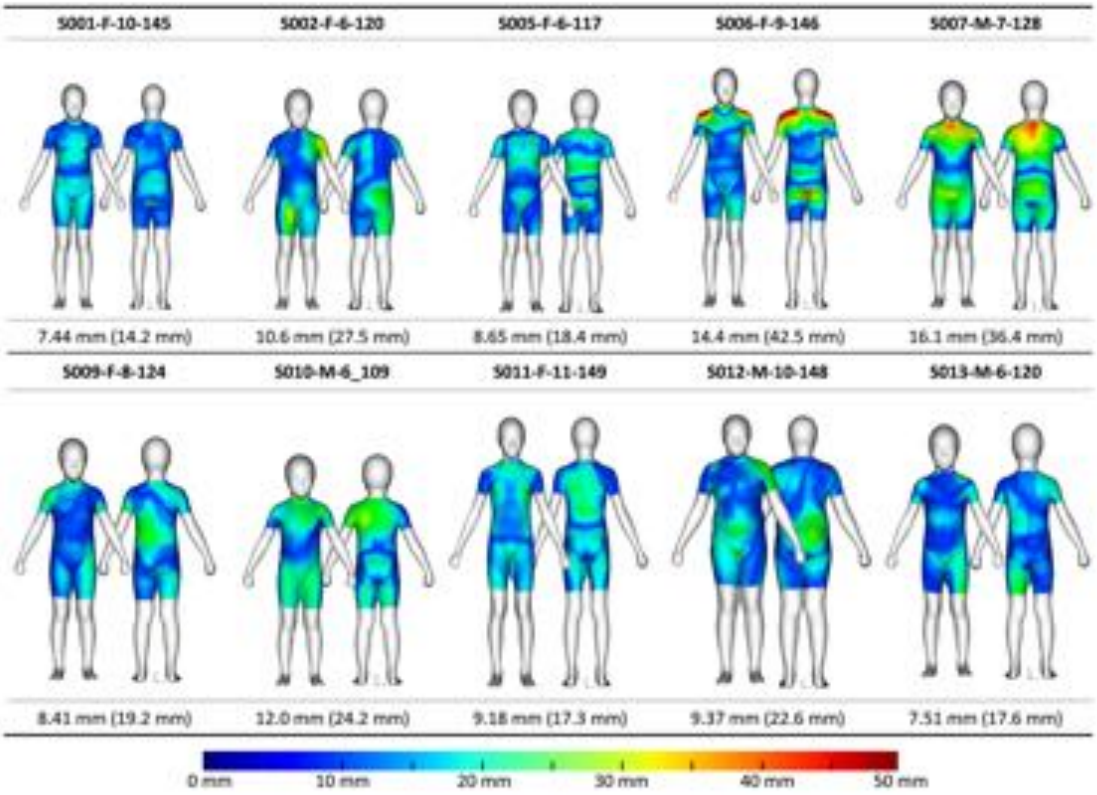

Figure 28. Comparisons between fitted template models and reconstructed data using anthropometric predictors such as stature, BMI, and SHS for 10 children.

Seated Body Shape Model

Figure 29 illustrates the effects of varying stature from 1100 to 1400 mm and BMI from 13 to 22 while holding posture at the mean. Figure 30 illustrates the effects of manipulating recline and flexion over the range in the data while holding the anthropometric variables at mean values.

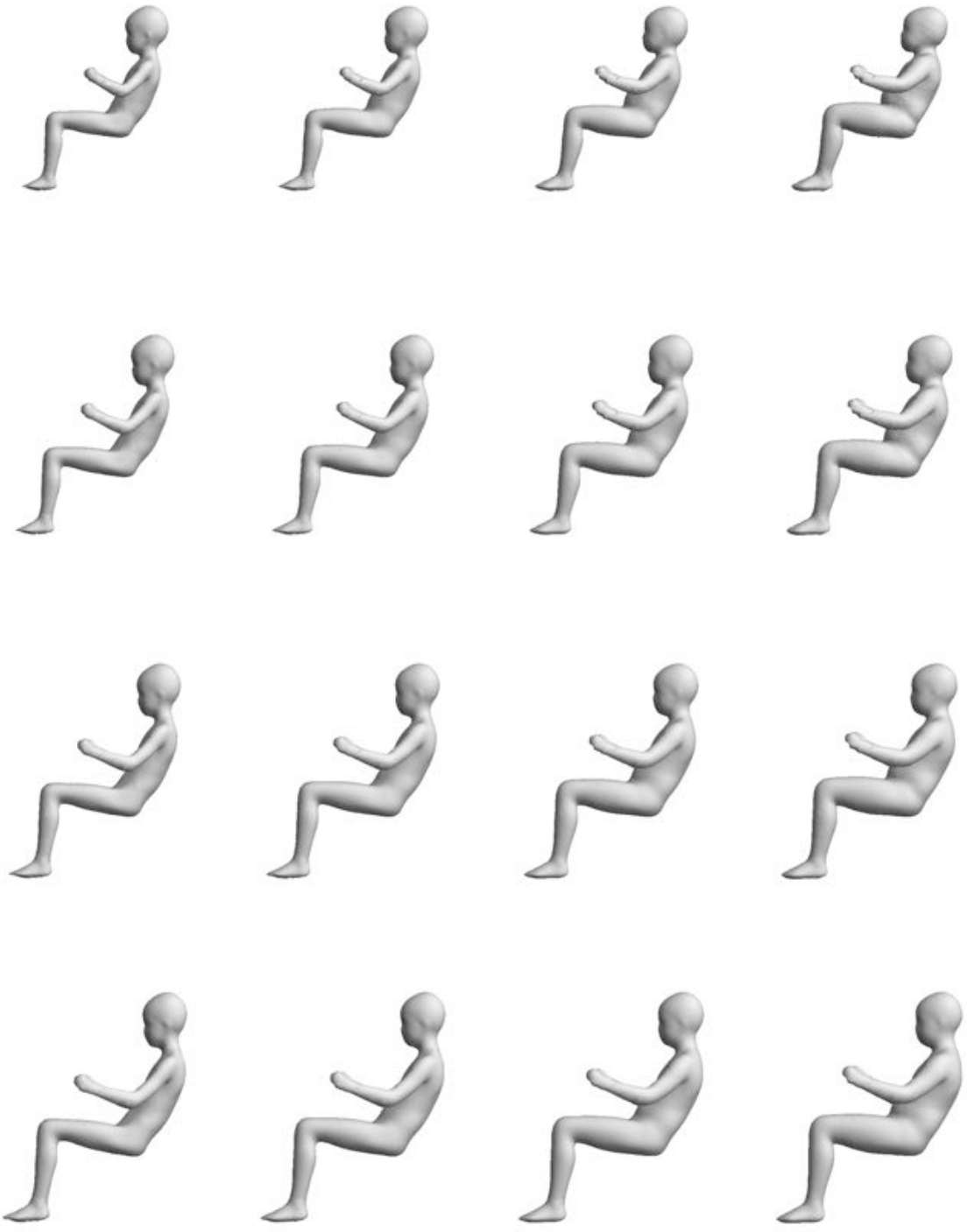

Figure 29. Sample output from the seated body shape model showing a range of stature (top to bottom) and body mass index (left to right).

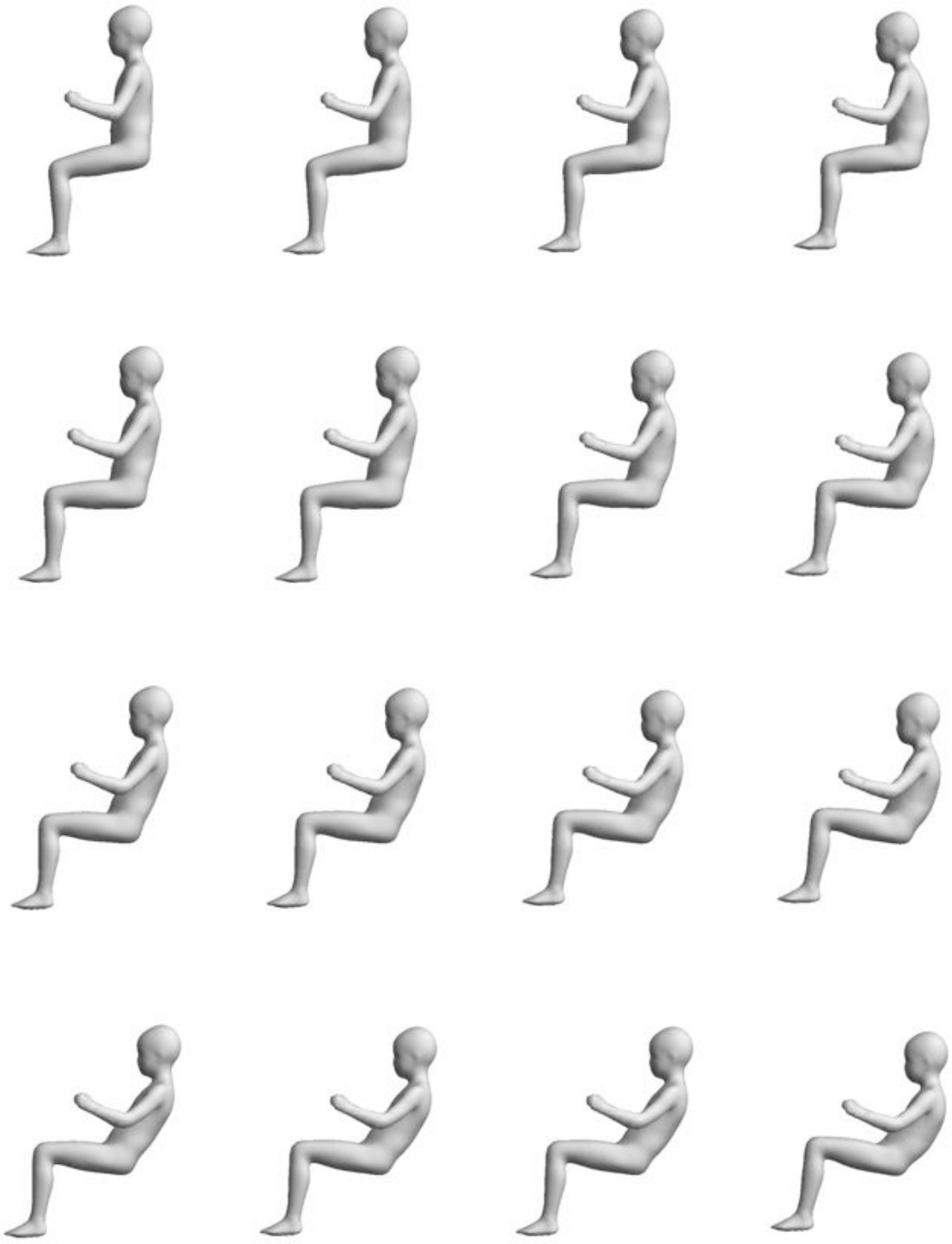

Figure 30. Sample output from the seated body shape model showing a range of recline (top to bottom) and lumbar flexion (left to right).

Comparison of Seated Model Predictions with ATD Body Shapes

Figure 31 compares the ATD shapes with manikin shapes predicted using the reference body dimensions of the ATD. The arms and legs were excluded in this comparison due to the pose difference. Unsigned errors between the two surfaces were coded with a color map representing 0 to 50 mm. Overall, the ATDs were found to be very similar in size to the model predictions, although some shape discrepancies were noted. The mean errors were 6.3 mm and 5.4 mm, and 95th %ile errors were 5.4 mm and 19.9 mm for 6YO and 10YO, respectively. Discrepancies in the head and neck were largely due to differences in neck posture. The largest differences were noted in the chest area, with the ATD chest deeper and more prominent in the upper chest.

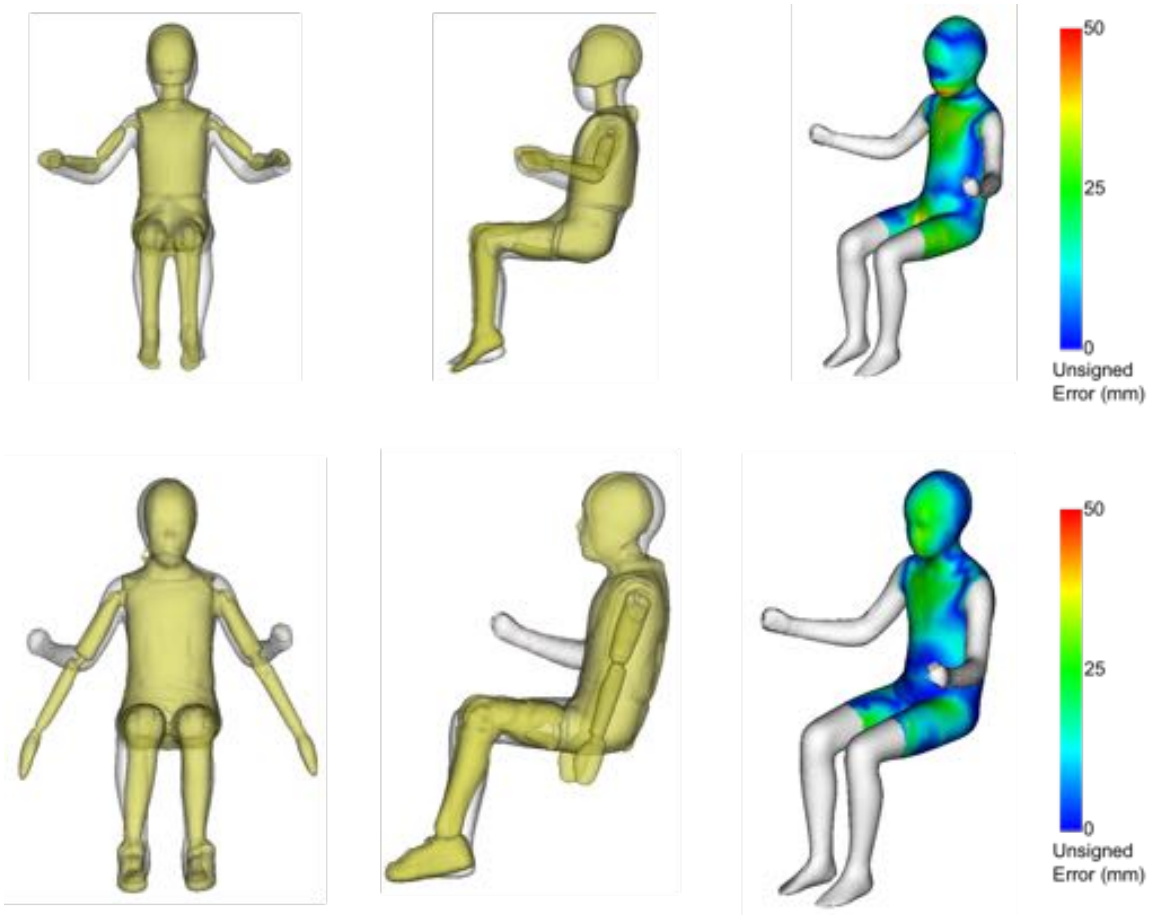

Figure 31. Comparison of the 6YO (upper) and 10 YO (lower) ATD shapes (yellow) to manikin shapes (white) predicted using the reference body dimensions of the ATD. Note that the upper extremities were not included in the fit or comparison.

Figure 32 compares the ATD shapes to manikin shapes obtained by fitting the SBSM to the scan data, in essence identifying the characteristics of the children that the ATDs most resemble. The mean distance discrepancies for the 6YO and 10YO were 5.0 mm

and 3.1 mm, and 95th %ile errors were 18.2 mm and 12.9 mm, respectively. The SBSM is able to predict standard anthropometric values based on the fit to each ATD scan.

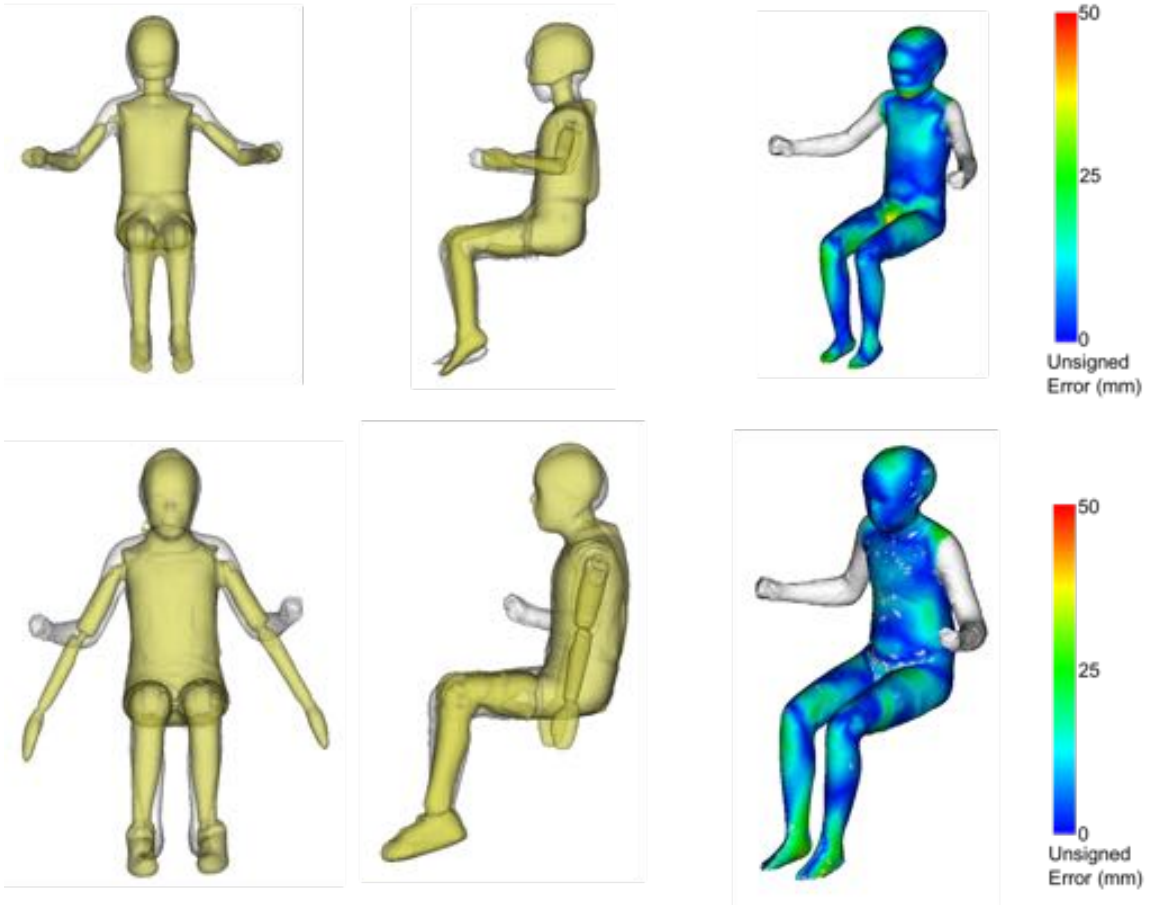

Figure 32. Comparison of the 6YO (top) and 10 YO (bottom) ATD shapes (yellow) to manikin shapes (white) fitted to each ATD shape. Note that the upper extremities were not included in the fit or comparison.

DISCUSSION

Achievements

This report describes the first large-scale, detailed study of the 3D anthropometry of U.S. children. A sample of 150 children ages 4 to 12 were measured using standard anthropometric methods as well as whole-body surface scanning and 3D landmark measurement. Unlike most anthropometric studies, the postures included supported seated postures relevant to vehicle occupant applications.

The data were analyzed using state-of-the-art techniques, including some methods new to this study, to obtain parametric models that predict body shape, surface landmark locations, and internal joint center locations as a function of overall body characteristics, such as stature and body weight. Two statistical body shape models were generated from the data: a model in a relaxed standing posture and a seated model capable of representing a range of recline and lumbar spine flexion. UMTRI has made these models available online (currently at http://childshape.org/ and http://childshape.org/seated/), providing a browser-based interface that allows specification of the overall body dimensions and downloading the resulting body surface shape, landmarks, and joints.

Applications

The rich data and models developed in this study will have broad application for vehicle safety and beyond. The proximate motivation for the study was to develop data and models suitable for evaluating and specifying the anthropometric characteristics of surrogates for representing child occupants. Physical ATDs are an important application, but the most widespread use will probably be in the specification of finite-element (FE) human body models (HBM) used to conduct crash simulations. UMTRI and others have developed methods for morphing FE HBMs to represent a wide range of occupant sizes and shapes (Hu et al. 2012, Beillas et al. 2015, Schoell et al. 2015). The data and models from the current study will enable current child FE HBMs to be extended to represent a much wider range of the population.

The data and models will also be useful for any other application for which the shape of children is important. These applications include design of child restraints, protective equipment, and medical devices worn on the body. New statistical models parameterized with different inputs, or based on different scanned postures, will be needed for some applications.

The statistical models are also useful for data acquisition applications in which human body shape is measured using less-accurate means than the laser scanners used in the current work. Park et al. (2014) developed a method for measuring child body shapes using Microsoft Kinect sensors. Fitting the relatively noisy and incomplete data using the standing body shape model reported in this work enabled accurate prediction of body dimensions and the creation of an avatar quickly, with inexpensive sensors. This method has been extended to create articulated mankins for ergonomics analysis using similar body shape models of adults (Reed et al. 2014). The seated model developed in the

current work has also been used in a pilot study to create an avatar from a Kinect scan of a person sitting in a vehicle seat, with potential applications to in-vehicle occupant monitoring (Park et al. 2015).

The data are also applicable to the development of improved body segment parameter data for children. Currently, estimates of segment masses, center-of-mass locations, and moments of inertia for children are based on simplistic assumptions regarding segment shape and volume. The newly developed models could be used to make much more refined estimates.

Limitations

As with all studies of its type, this study is limited by the characteristics of the sample. Although 150 children represents the largest study to date of 3D anthropometry on U.S. children, the sample is not representative of the distribution of race and ethnicity in the U.S. In particular, Black and Hispanic children are substantially underrepresented. The sample also does not include a large number of children with high BMI. Because such children may be at increased risk of being disaccommodated by vehicle restraint systems, more data from these populations are needed.

This sample and the resulting models are limited to children in the age range from approximately 3 to 12 years. The models are likely to be accurate down to typical body dimensions of 3YO children, but extrapolating above the mean size of 12YO children is not recommended due to the differential effects of puberty on boys and girls. Limiting the model to pre-pubescent children allowed the creation of a unisex model, but future studies should include sex-specific models of adolescents. Large amounts of adult data are already available, but further data collection is needed on children ages 12 to 18 years. In a recent study, UMTRI gathered data and modeled body shapes for children ages 12 to 36 months, filling the "toddler" gap at ages below those in the current study (Kim et al. 2015). Additional data on infants may be warranted, but gathering data for recumbent children not capable of maintaining prescribed postures is challenging (Ebert et al. 2014).

The scan data have some important limitations. In particular, the hands, feet, and heads are not well represented. The scanner does not have sufficient resolution to scan hands and feet accurately, and the head shapes are distorted by the swim caps used to contain the participants' hair. Consequently, the data are not suitable for some design applications that require accurate head shape information, such as helmet design.

The current data analysis and modeling approaches have some limitations that should be addressed in future work. All methods for template fitting to shape data tend to result in smoothing when further statistical analyses are conducted, because they are not homologous at all vertices. The methods used for the current work ensured that the fitted meshes were homologous at several dozen landmark locations, but shapes between landmarks will tend to be smoothed when multiple fitted scans are averaged. Consequently, the output of the regression models will generally be smoother, with fewer high-resolution features, than any individual scan. In general, the consequences of this smoothing and suitable alternative modeling approaches are application-dependent. For

example, an application that required detailed face shape information would necessitate the use of more face landmarks when performing template fitting. In general, the methods chosen for the current analysis are believed to be appropriate for the intended applications in whole-body human surrogate development for crash safety applications.

The modeling methods used in this study do not separately parameterize posture (pose) and body shape. Further, the analysis is conducted without explicit consideration of the underlying kinematic linkage. This approach produces a simpler model that is more readily implemented, but the ability to specify the posture of the model is substantially limited. The standing model has no posture parameterization. The seated model has two degrees of freedom affecting torso posture, which gives it the ability to represent a wide range of vehicle-relevant postures. This approach is arguably superior to a kinematic approach to torso modeling, because the kinematic approach requires modeling the complex changes in torso posture as a function of linkage variables. The regression-based approach used for the current seated model is limited in that it cannot be readily extended to handle extremity postures, but it is likely the simplest method capable of producing a wide range of accurate torso shapes.

Many other model formulations can be generated from the template-fitted data to serve various purposes. For example, the body shape can be predicted from a combination of overall body dimensions (stature, body weight, etc.) and the locations of particular landmarks (Reed 2013a). Recently this method was used to develop an adult ATD body form, ensuring that the body form matched the target landmark and joint locations (Reed 2013b).

Future Work

Future studies should expand the study sample, with a particular focus on minority and high-BMI children. Advancements in modeling methods are also needed so that a larger amount of the data gathered in this study can be utilized. Specifically, a fully posable model based on a kinematic linkage is needed to enable modeling of the wide range of torso and upper-extremity postures recorded in the study. A similar study of adolescent children ages 12 to 18 is also needed.

REFERENCES

Beillas, P., Petit, P., Kleiven, S., Kirscht, S., Chawla, A., Jolivet, E., Faure, F., Praxl, N., and Bhaskar, A., (2015). Specifications of a software framework to position and personalize human body models. *Proc. IRCOBI Conference*, Lyon, France.

Ebert S.M., Klinich K.D., Manary, M.A., Malik, L.M., and Reed, M.P. (2014). Toddler Lower Extremity Posture in Child Restraint Systems. UMTRI-2014-8. University of Michigan Transportation Research Institute, Ann Arbor, MI.

Gordon, C. C., Churchill, T., Clauser, C. E., Bradtmiller, B., McConville, J. T., Tebbetts, I., and Walker, R. A. (1989). 1988 Anthropometric Survey of U.S. Army Personnel: Methods and Summary Statistics. Final Report. (NATICK/TR-89/027). U.S. Army Natick RDEC.

Gordon, C.C., Blackwell, C.L., Bradtmiller, B., Parham, J.L., Barrientos, P., Pacquette, S.P., Corner, B.D., Carson, J.M., Venezia, J.Z., Rockwell, B.M., Mucher, M., and Kristensen, S. (2015). 2012 Anthropometric Survey of U.S. Army Personnel: Methods and Summary Statistics. Technical Report NATICK/TR-15/007. U.S. Army Natick Soldier Research, Development and Engineering Center Natick, Massachusetts.

Hu, J., Rupp, J.D., and Reed, M.P. (2012). Focusing on vulnerable populations in crashes: recent advances in finite element human models for injury biomechanics research. *Journal of Automotive Safety and Energy*, 3(4):295-307.

Huang, S. and Reed, M.P. (2006). Comparison of child body dimensions with rear seat geometry. *SAE Transactions: Journal of Passenger Cars – Mechanical Systems,* 115:1078-1087.

Mertz, H.J., Jarrett, K., Moss, S., Salloum, M., and Zhou, Y. (2010). The Hybrid-III 10-Year-Old Dummy. *Proceedings of the 45th Stapp Car Crash Conference.* SAE International, Warrendale, PA.

Kim, K.H., Jones, M.L.H., Ebert, S.M., Malik, L., Manary, M.A., Reed, M.P., and Klinich, K.D. (2015). Development of Virtual Toddler Fit Models for Child Safety Restraint Design. Technical Report UMTRI-2015-38. University of Michigan Transportation Research Institute, Ann Arbor, MI.

Klein, K.F., Hu, J., Reed, M.P., Hoff, C.N., and Rupp, J.D. (2015). Development and validation of statistical models of femur geometry for use with parametric finite element models. *Annals of Biomedical Engineering,* 43(10): 2503-2514. 10.1007/s10439-015-1307-6

Park, B-K, Lumeng, J.C., Lumeng, C.N., Ebert, S.M., and Reed, M.P. (2014). Child body shape measurement using depth cameras and a statistical body shape model. *Ergonomics,* 58(2):301-309. 10.1080/00140139.2014.965754

Park, B.-K., Ebert, S.M., Kim, H.K., and Reed, M.P. (2015). A Pilot Study of In-Vehicle Posture Tracking Using Depth Cameras. Technical Report UMTRI-2015-42. University of Michigan Transportation Research Institute, Ann Arbor, MI.

Park, B-K and Reed, M.P. (2015). Parametric body shape model of standing children ages 3 to 11 years. *Ergonomics*, 58(10):1714-1725. 10.1080/00140139.2015.1033480

Reed, M.P., Manary, M.A., and Schneider, L.W. (1999). Methods for measuring and representing automobile occupant posture. Technical Paper 990959. Society of Automotive Engineers, Warrendale, PA.

Reed, M.P., Lehto, M.M., Schneider, L.W., Moss, S., Nghi, T. (2001). Development of anthropometric specifications for the six-year-old OCATD. *SAE Transactions: Journal of Passenger Cars — Mechanical Systems,* 110: 497-504.

Reed, M.P., Ebert-Hamilton, S.M., Manary, M.A., Klinich, K.D., and Schneider, L.W. (2005). A new database of child anthropometry and seated posture for automotive safety applications. *SAE Transactions: Journal of Passenger Cars - Mechanical Systems,* 114: 2222-2235.

Reed, M.P., Ebert-Hamilton, S.M., Manary, M.A., Klinich, K.D., and Schneider, L.W. (2006). Improved positioning procedures for 6YO and 10YO ATDs based on child occupant postures. *Stapp Car Crash Journal*, 50: 337-388.

Reed, M.P. and Parkinson, M.B. (2008). Modeling variability in torso shape for chair and seat design. DETC2008-49483. *Proceedings of the ASME Design Engineering Technical Conferences.* ASME, New York.

Reed, M.P., Ebert-Hamilton, S.M., Klinich, K.D., Manary, M.A., and Rupp, J.D. (2008). Assessing Child Belt Fit, Volume I: Effects of Vehicle Seat and Belt Geometry on Belt Fit for Children with and without Belt Positioning Booster Seats. Technical Report UMTRI-2008-49-1. University of Michigan Transportation Research Institute, Ann Arbor, MI.

Reed, M.P., Ebert, S.M., Sherwood, C.P., Klinich, K.D., and Manary, M.A. (2009a). Evaluation of the static belt fit provided by belt-positioning boosters. *Accident Analysis and Prevention*, 41:598-607.

Reed, M.P., Sochor, M.M., Rupp, J.D., Klinich, K.D., and Manary, M.A. (2009b). Anthropometric specification of child crash dummy pelves through statistical analysis of skeletal geometry. *Journal of Biomechanics,* 42:1143-1145.

Reed, M.P. (2013a). Modeling body shape from surface landmark configurations. *Human Modeling and Applications in Health, Safety, Ergonomics, and Risk Management. Human Body Modeling and Ergonomics. Lecture Notes in Computer Science,* 8026:376-383.

Reed, M.P. (2013b). Development of Anthropometric Specifications for the Warrior Injury Assessment Manikin (WIAMan). Technical Report UMTRI-2013-38. University of Michigan Transportation Research Institute, Ann Arbor, MI.

Reed, M.P., Ebert-Hamilton, S.M., Klinich, K.D., Manary, M.A., and Rupp, J.D. (2013). Effects of vehicle seat and belt geometry on belt fit for children with and without belt positioning booster seats. *Accident Analysis and Prevention.* 50:512-22. 10.1016/j.aap.2012.05.030

Reed, M.P., Byoung-Keon, P., Kim, K.H., and Raschke, U. (2014). Creating custom avatars for ergonomic analysis using depth cameras. *Proceedings of the 2014 Human Factors and Ergonomics Society Annual Meeting.* HFES, Santa Monica, CA.

Reynolds, H. M., Young, J. W., McConville, J. T., and Snyder, R. G. (1976). Development and evaluation of masterbody forms for three-year old and six-year old child dummies. Final Report No. DOT/HS 801 811. Washington, D.C.: National Highway Traffic Safety Administration.

Robinette, K. M., Daanen, H., & Paquet, E. (1999). The CAESAR project: a 3-D surface anthropometry survey. In *3-D Digital Imaging and Modeling*, Second International Conference on (pp. 380-386). IEEE.

Schoell, S.L., Weaver, A.A., Urban, J.E., Jones, D.A., Stitzel, J.D., Hwang, E., Reed, M.P., and Rupp, J.D. (2015). Development and validation of an older occupant finite element model of a mid-sized male for investigation of age-related injury risk. *Stapp Car Crash Journal*, 59:359-383

Shi, X., Hu, J., Reed, M.P., Rupp, J.D., Hoff, C.N. and Cao, L. (2014). A Statistical human rib cage geometry model accounting for variations by age, sex, stature and body mass index. *Journal of Biomechanics*. 47(10):2277-2285. 10.1016/j.jbiomech.2014.04.045

Snyder, R.G., Schneider, L.W., Owings, C.L., Reynolds, H.M., Golumb, D.H., and Schork, M.A. (1977). Anthropometry of Infants, Children, and Youths to Age 18 for Product Safety Design. Final Report UM-HSRI-77-17. University of Michigan Transportation Research Institute, Ann Arbor, MI.

APPENDIX A
Description of Surface Markers

Point Name	Body Part	Additional Description	Point to Digitize
Head3_M	Head	About 1" above glabella, on skin that doesn't move when raising eye brows, not covered by swim cap	Superior, Subject's Left
Head2_M	Head	On or above left cheek bone about 1" anterior to tragion	Superior-Posterior
Head1_M	Head	On or above right cheek bone about 1" anterior to tragion	Superior-Posterior
AcromionLt_H	Torso	Center of hemisphere on most anterior point on the acromion	Center of hemisphere
AcromionRt_H	Torso	Center of hemisphere on most anterior point on the acromion	Center of hemisphere
ElbowMedLt_M	Arm	Medial epicondyle (mark with elbow bent 45°)	Proximal, extensor surface
ElbowMedRt_M	Arm	Medial humeral epicondyle (mark with elbow bent 45°)	Proximal, extensor surface
ElbowLatLt_M	Arm	Lateral epicondyle (mark with elbow bent 45°)	Proximal, extensor surface
ElbowLatRt_M	Arm	Lateral humeral epicondyle (mark with elbow bent 45°)	Proximal, extensor surface
WristMidTopLt_M	Arm	On the back of the wrist slightly proximal to the cross section plane of the ulnar styloid.	Proximal, nearest Ulnar Styloid
WristMidTopRt_M	Arm	On the back of the wrist slightly proximal to the cross section plane of the ulnar styloid.	Proximal, nearest Ulnar Styloid
WristBotTopLt_M	Arm	On the palm side of the wrist opposite the wrist mid marker	Proximal, nearest Ulnar Styloid
WristBotTopRt_M	Arm	On the palm side of the wrist opposite the wrist mid marker	Proximal, nearest Ulnar Styloid
SpineC07_M	Torso	Spinous process of the 7th cervical vertebra (cervicale)	Center
SpineT04_M	Torso	Spinous process of 4th thoracic vertebra	Center
SpineT08_M	Torso	Spinous process of 8th thoracic vertebra	Center
SpineT12_M	Torso	Spinous process of 12th thoracic vertebra	Center
SpineL01_M	Torso	Spinous process of 1st lumbar vertebra	Center
SpineL02_M	Torso	Spinous process of 2nd lumbar vertebra	Center
SpineL03_M	Torso	Spinous process of 3rd lumbar vertebra	Center
SpineL04_M	Torso	Spinous process of 4^{d} lumbar vertebra	Center
SpineL05_M	Torso	Spinous process of 5th lumbar vertebra	Center
10RibLt_M	Torso	Most lateral point on the 10th rib	Superior-Posterior
10RibRt_M	Torso	Most lateral point on the 10th rib	Superior-Posterior
L3Position_M	Torso		
IlioRt_M	Torso	Iliocristale (most superior lateral point on pelvis when standing	Superior-Posterior
IlioLt_M	Torso	Iliocristale (most superior lateral point on pelvis when standing	Superior-Posterior
ChestUpper_M	Torso	Body midline, about one thumb's width down from suprasternale, (or about mid-manubrium)	Superior, Subject's Left
ChestLower_M	Torso	Body midline, first flat, boney surface on sternum body above belly	Superior, Subject's Left
TorsoLt_M	Torso	Midpoint between 10th rib and iliocristale point	Superior-Posterior
TorsoRt_M	Torso	Midpoint between 10th rib and iliocristale point	Superior-Posterior
TorsoMid1_M	Torso	Between TorsoMid2 and substernale	Superior, Subject's Left
TorsoMid2_M	Torso	Above umbilicus	Superior, Subject's Left

KneeFemMedLt_M	Leg	Femoral epicondyle, medial	Proximal, flexor surface
KneeFemMedRt_M	Leg	Femoral epicondyle, medial	Proximal, flexor surface
KneeFemLatLt_M	Leg	Femoral epicondyle, lateral	Proximal, flexor surface
KneeFemLatRt_M	Leg	Femoral epicondyle, lateral	Proximal, flexor surface
AnkleMedLt_M	Leg	Malleolus, medial	Proximal, plantar flexion surface side
AnkleMedRt_M	Leg	Malleolus, medial	Proximal, plantar flexion surface side
AnkleLatLt_M	Leg	Malleolus, lateral	Proximal, plantar flexion surface side
AnkleLatRt_M	Leg	Malleolus, lateral	Proximal, plantar flexion surface side

APPENDIX B
Description of Landmarks Digitized on Scans

Point Name	Body Part	Additional Description
HeadTopCt_L	Head	Most superior point on head or helmet
HeadBackCt_L	Head	Most posterior point on head or helmet
HeadTragLt_L	Head	Notch just above the tragus of the ear
EyeCorLt_L	Head	Point on orbit nearest the corner of eye
EyeCenLt_L	Head	Point on orbit below the eye at the same lateral position as the pupil when looking straight forward
HeadGlabCt_L	Head	Glabella: Smooth elevation of the frontal bone just above the bridge of the nose, between eyebrows
EyeCenRt_L	Head	Point on orbit below the eye at the same lateral position as the pupil when looking straight forward
EyeCorRt_L	Head	Point on orbit nearest the corner of eye
HeadTragRt_L	Head	Notch just above the tragus of the ear
NoseTipCt_L	Head	Tip of nose
ChinTipCt_L	Head	Menton (tip of chin)
WristLatLt_L	Arm	Styloid process on ulna(pinky side) – opposite of wrist "bump"
WristLatRt_L	Arm	Styloid process on ulna (pinky side) lateral point on wrist "bump"
WristMedLt_L	Arm	Styloid process on radius (thumb side) – opposite of wrist "bump"
WristMedRt_L	Arm	Styloid process on radius (thumb side) lateral point on wrist "bump"
Mcar5LatRt_L	Arm	Knuckle – grip axis, pinky side (5^{th} metacarpal medial)
Mcar2MedRt_L	Arm	Knuckle – grip axis, index side
Mcar2MedLt_L	Arm	Knuckle – grip axis, pinky side
Mcar5LatLt_L	Arm	Knuckle – grip axis, index side
SternSupCt_L	Torso	Anterior surface of jugular notch
SternSubCt_E	Torso	Substernale
InnerThighCt_E	Torso	Most inferior midline point on torso – mid crotch point
ThighJnctRtLat_L	Torso	Thigh – abdominal junction, lateral point (defining a line)
ThighJnctRtMed_L	Torso	Thigh – abdominal junction, medial point (defining a line)
ThighJnctLtMed_L	Torso	Thigh – abdominal junction, medial point (defining a line)
ThighJnctLtLat_L	Torso	Thigh – abdominal junction, lateral point (defining a line)
AxillaLtFt_L	Torso	Armpit Front (anatomical – not where the scan separates)
AxillaRtFt_L	Torso	Armpit Front
AxillaRtRr_L	Torso	Armpit Rear
AxillaLtRr_L	Torso	Armpit Rear
CenterButtocks_E	Torso	Most posterior midline point on the buttocks
FootMtar5LatLt_L	Leg	Ball of foot lateral (metatarsal-phalangeal protrusion)
FootMtar5LatRt_L	Leg	Ball of foot lateral
FootMtar1MedLt_L	Leg	Ball of foot medial
FootMtar1MedRt_L	Leg	Ball of foot medial
FootToe1Lt_L	Leg	Acropodian (most distal phalangeal point)
FootToe1Rt_L	Leg	Acropodian (most distal phalangeal point)
FootHeelRt_L	Leg	Most posterior point on right heel
FootHeelLt_L	Leg	Most posterior point on left heel
KneeSupLt_L	Leg	Most proximal point on left patella
KneeInfLt_L	Leg	Most distal point on left patella
KneeSupRt_L	Leg	Most proximal point on right patella
KneeInfRt_L	Leg	Most distal point on right patella